WSRC-TR-97-0120

VAPOR CORROSION OF ALUMINUM CLADDING ALLOYS AND ALUMINUM-URANIUM FUEL MATERIALS IN STORAGE ENVIRONMENTS (U)

P. S. Lam
R. L. Sindelar
H. B. Peacock, Jr.

Savannah River Technology Center
Strategic Materials Technology Department
Materials Technology Section

Publication Date: April 1997

Westinghouse Savannah River Company
Savannah River Site
Aiken, SC 29808

This document was prepared in connection with work done under Contract No. DE-AC09-96SR18500 with the U. S. Department of Energy

DOCUMENT: WSRC-TR-97-0120

TITLE: VAPOR CORROSION OF ALUMINUM CLADDING ALLOYS AND ALUMINUM-URANIUM FUEL MATERIALS IN STORAGE ENVIRONMENTS (U)

TASK: SRT-MTS-96-2041, Rev. 1, Task 2.1

APPROVALS

P.S. Lam

Date: 4-30-97

Poh-Sang Lam, Lead Author
Materials Applications & Corrosion Technology Group
MATERIALS TECHNOLOGY SECTION

P. E. Zapp

Date: 4-30-97

P. E. Zapp, Technical Reviewer
Materials Applications & Corrosion Technology Group
MATERIALS TECHNOLOGY SECTION

N. C. Iyer

Date: 4/30/97

N. C. Iyer, SRTC-Spent Nuclear Fuel Manager
Materials Applications & Corrosion Technology Group
MATERIALS TECHNOLOGY SECTION

T. L. Capeletti

Date: 4/30/97

T. L. Capeletti, Manager
MATERIALS TECHNOLOGY SECTION

J. R. Murphy

Date: 4/30/97

J. R. Murphy
SPENT FUEL STORAGE DIVISION

(Blank Page)

TABLE OF CONTENTS

LIST OF TABLES

LIST OF FIGURES

LIST OF ACRONYMS

Acronym	Definition
Al SNF	Aluminum-clad, aluminum-based Spent Nuclear Fuel
ANL	Argonne National Laboratory
ANSI/ANS	American National Standards Institute/American Nuclear Society
ASME	American Society of Mechanical Engineers
ATR	Advanced Test Reactor
ATTP	Alternative Al SNF Treatment Technology Program
ASTM	American Society for Testing and Materials
CPP	Chemical Processing Plant (INEL)
EIS	Environmental Impact Statement
DOE-EM	U.S. Department of Energy Office of Environmental Management
DOE-RW	U.S. Department of Energy Office of Civilian Radioactive Waste Management (also OCRWM)
DRR	Domestic Research Reactor
F&OR	Functional & Operating Requirements
FRR	Foreign Research Reactor
HEDL	Hanford Engineering Development Laboratory
HEU	Highly-Enriched Uranium (> 20% U-235 in U)
HFIR	High Flux Isotope Reactor
HLW	High Level Waste
ICPES	Inductively Coupled Plasma Emission Spectroscopy
IMNM	Interim Management of Nuclear Materials
INEL	Idaho National Engineering Laboratory
LANL	Los Alamos National Laboratory
LEU	Low-Enriched Uranium (2 to 20% U-235 in U)
LLNL	Lawrence Livermore National Laboratory
MCO	Multi-Canister Overpacks
MPC	Multi-Purpose Canister
MRS	Monitored Retrievable Storage
MTR	Materials Test Reactor
MTRE	Materials Test Reactor Equivalent
NDE	Non-Destructive Examination
NRC	Nuclear Regulatory Commission
ORNL	Oak Ridge National Laboratory
PEIS	Programmatic Environmental Impact Statement
PNNL	Pacific Northwest National Laboratory
RBOF	Receiving Basin for Offsite Fuel
RH	Relative Humidity (vapor pressure of H_2O/saturation pressure of H_2O)
SCC	Stress Corrosion Cracking
SEM	Scanning Electron Microscope
SI	Structural Integrity
SNF	Spent Nuclear Fuel
SRS	Savannah River Site
TMI	Three Mile Island
SRTC	Savannah River Technology Center
VLEU	Very-Low-Enriched Uranium (< 2% U-235 in U)

(Blank Page)

1.0 SUMMARY

An experimental investigation of the effects of vapor environments on the corrosion of aluminum spent nuclear fuel (Al SNF) has been performed. Aluminum cladding alloys and aluminum-uranium fuel alloys have been exposed to environments of air/water vapor/ionizing radiation and characterized for applications to degradation mode analysis for interim dry and repository storage systems. Models have been developed to allow predictions of the corrosion response under conditions of unlimited corrodant species. Threshold levels of water vapor under which corrosion does not occur have been identified through tests under conditions of limited corrodant species.

Coupons of aluminum-1100, 5052, and 6061, the U.S. equivalent of cladding alloys used to manufacture foreign research reactor fuels, and several aluminum-uranium alloys (aluminum-10, 18, and 33 wt% uranium) were exposed to various controlled vapor environments in air within the following ranges of conditions :

Temperature:	80 to 200°C
Relative Humidity:	0 to 100% using atmospheric condensate water and using added nitric acid to simulate radiolysis effects.
Gamma Radiation:	None and 1.8×10^6 R/hr

Corrosion of all the alloys occurred initially by parabolic growth in thickness of a film of boehmite, $Al_2O_3 \cdot H_2O$. A marked post-parabolic regime was observed in the corrosion response of aluminum 5052 which corresponds to the onset of internal oxidation. Mechanistically-based, empirical models were developed for each of the aluminum cladding alloys to describe the conversion of metal to oxide with exposure time. The models are in the following form:

$$\text{weight gain} = A \cdot \exp(-Q_1/RT) \cdot t^n \qquad \text{(parabolic regime)}$$

$$\text{weight gain} = B_0 + B_1 \cdot \exp(-Q_2/RT) \cdot t \text{(post-parabolic regime).}$$

A temperature-dependent threshold in the critical relative humidity necessary for the corrosion of the cladding alloys was observed. The critical humidity at room temperature reported in the literature is between 40 to 70% whereas results at 150°C in the present investigation suggest a threshold at approximately 20% relative humidity. In the presence of the radiation field, corrosion occurred at every humidity condition and no critical level of relative humidity was observed.

The corrosion results and models can be generally applied to predict the degradation of fuel materials in sealed and non-sealed (e.g. breached container) storage environments. In a sealed system containing finite amounts of water vapor, the rate of corrosion slows with time to less than the parabolic rate for unlimited species. The corrosion reactions stop after water is consumed down to the critical relative humidity level. Equations are also developed to allow calculation of the amount of hydrogen and its partial pressure in a sealed system.

The corrosion of the aluminum-uranium fuel materials initially occurs at rates up to several times that for the aluminum cladding alloys, followed by a region of corrosion at rates similar to the cladding alloys. A dependence on the amount and distribution of the uranium aluminides in the aluminum-uranium alloy appears to cause the variability in the

initial corrosion rates. Blistering of the metal matrix is observed at several localized regions and is attributed to hydrogen evolved at high rates. The uranium aluminide particles, observed in the oxide film, appear to be chemically stable under the test conditions while the aluminum matrix converts to boehmite.

The results of this work are part of the body of information needed for understanding the degradation of the Al SNF waste form in a direct disposal system in the federal repository. It will provide the basis for data input to the ongoing performance assessment and criticality safety analyses. Additional testing is being initiated to include the J-13 water chemistry (well water of the repository site in Yucca Mountain) and modified J-13 water (J-13 water altered by dissolution of waste package and waste form materials) as the water source for the vapor to evaluate the effects of impurities on the corrosion mode and rates. Additional testing of uranium-aluminum fuel materials at uranium contents typical of high enriched and low enriched fuels is being initiated to provide the data needed for the development of empirical models.

2.0 INTRODUCTION

The Office of Civilian Radioactive Waste Management of the Department of Energy (DOE-RW) is presently in the process of qualifying the Defense High Level Waste (HLW) and commercial spent nuclear fuel (SNF) for storage in the federal repository. Alternatives to the disposition of spent nuclear fuel currently under the jurisdiction of the Office of Environmental Management (DOE-EM) include direct disposal, or co-disposal with the HLW, in the repository waste package. The scope of waste forms for the repository has thus recently been expanded to include the DOE-EM fuels which include aluminum-based SNF (Al SNF) from foreign and domestic research reactors (FRR and DRR, respectively).

Qualification for storage in the repository includes three activities:

1) Total System Performance Assessment;

2) Criticality Analysis; and

3) Technical Package Development for Licensing of the Repository by the U. S. Nuclear Regulatory Commission (NRC)

An experimental and analytical program is being conducted at the Savannah River Technology Center (SRTC) to develop the technologies to enable the interim storage of aluminum-based SNF "road-ready" in a dry storage system at the Savannah River Site (SRS) followed by ultimate disposition in a direct disposal system in the federal repository. The activities in this program include studies to develop information on materials' response under potential storage conditions and to develop mathematical models of the degradation processes for input to the repository performance assessment, criticality analyses, and licensing package.

Vapor corrosion is the primary degradation mode of Al SNF under direct disposal storage. The corrosion program to quantify rates and model the response to a range of vapor conditions is described in this report. Empirical models have been developed for the corrosion response of the cladding materials. Several results have also been obtained from initial vapor corrosion tests of aluminum-uranium fuel materials.

Aluminum alloys 1100, 5052, and 6061 were chosen for the corrosion tests because their chemical compositions are similar to those of most of the FRR/DRR cladding alloys. The composition of the coupon specimens used in the test program is within the specified compositions. The compositions are listed in Table 1.

Table 1 - Aluminum Alloy Compositions

AL-Alloy (#100 Ser.)	Si	Fe	Cu	Mn	Cr	Ni	Zn	Ti	V	Ga	Zr	Sn	Pb	Mg	Bi	Al	Total
	wt%	wt%	wt%	wt%	wt%	wt%	wt%	wt%	wt%	wt%	wt%	wt%	wt%	wt%	wt%	wt%	wt%
1100	0.104	0.521	0.128	0.005	0.007	0.009	0.009	0.007	0.008	0.011	0.000	0.000	0.000	0.012	0.000	99.18	100
5052	0.116	0.284	0.014	0.022	0.188	0.012	0.011	0.019	0.012	0.013	0.001	0.000	0.000	2.522	0.000	96.79	100
6061	0.613	0.497	0.300	0.031	0.228	0.012	0.024	0.012	0.016	0.012	0.000	0.000	0.000	1.019	0.000	97.24	100

The following environmental exposure conditions have been investigated:

(i) The cladding materials are subject to unlimited corrodant species (water vapor only and water vapor with nitric acid to simulate radiolysis effects) at elevated temperatures. The tests were carried out in an autoclave.

(ii) The cladding materials are subject to limited corrodant species (water vapor only and water vapor with nitric acid to simulate radiolysis effects) at elevated temperatures. The tests were carried out with specimens enclosed in specially designed stainless steel capsules placed in ovens.

(iii) The cladding materials are subject to limited corrodant species (water vapor) and exposed to a cobalt 60 high radiation source (~2,000,000 R/hr) at elevated temperatures. The tests were carried out with specimens enclosed in stainless steel capsules placed in a cobalt-60 gamma cell.

In addition, preliminary water vapor corrosion tests for a fuel material (aluminum-10 wt% uranium) have been carried out. Some sections of aluminum-8001-clad fuel material of Al-18, -33% depleted uranium were also tested for general and pitting corrosion under water vapor environments.

Models for the corrosion of aluminum cladding alloys were developed and benchmarked by the corrosion test results. The corrosion models, along with the aluminum oxidation chemical balance equation, allow the estimation of hydrogen generation in a closed system.

Section 3 of this report describes the corrosion testing, results, and models for aluminum cladding alloys in unlimited vapor conditions. Section 4 describes the testing and results for the cladding alloys in vapor conditions of limited corrodant species and no radiation. Section 5 describes the testing and results for the cladding alloys in vapor conditions of limited corrodant species under gamma radiation. Section 6 provides an assessment of the mechanisms controlling the corrosion of the aluminum cladding alloys. Sections 7 and 8 describe the corrosion testing to date and the results for the aluminum-uranium fuel materials. Section 9 provides the framework for calculating hydrogen build-up in a sealed canister. Section 10 provides an overview of the application of the vapor

corrosion test results to the storage of Al SNF. Section 11 identifies additional vapor corrosion information needed and the tests being planned in the vapor corrosion program.

The full set of test data used in the following sections is retained in the laboratory record books for this task.

3.0 VAPOR CORROSION OF ALUMINUM CLADDING ALLOYS - UNLIMITED CORRODANT

The source of water for the "unlimited" water vapor tests was atmospheric condensate at the Savannah River Site. The water was obtained using a condensing coil and collected in polyethylene bottles. Water samples were submitted to the analytical laboratories at SRTC for chemical analysis. Chemical analysis for elemental impurity species was performed using inductively coupled plasma emission spectroscopy. Anion analysis was done by ion chromatography. The results for major elements are given in Table 2 along with the pH and conductivity results. The water samples were also submitted for analysis after each run in the autoclave. Table 3 summarizes these results.

Table 2 - Condensate Water Chemical Analysis

pH	5.89 - 7.944
Conductivity	12 to 53 µS/cm
Chloride	0.446 - 3.56 µg/ml
Fluoride	< 0.2 µg/ml
Nitrate	< 1.5 µg/ml
Nitrite	< 1 µg/ml
Sulphate	1.36 - 7.67 µg/ml
Ca	0.577- 4.501 µg/ml
Mg	0.198 - 0.435 µg/ml
Al	< 0.010 - 0.325 µg/ml
Fe	0.006 - 0.083 µg/ml
Na	1.076 - 7.891 µg/ml

Table 3 - Water Chemical Analysis Post-Test

pH	4.84 - 7.79
Conductivity	96 to 384 µS/cm
Chloride	8.29 - 41.6 µg/ml
Fluoride	< 20 µg/ml
Nitrate	< 150 µg/ml
Nitrite	< 100 µg/ml
Sulphate	12.8 - 55.1 µg/ml
Ca	2.140 - 22.174 µg/ml
Mg	0.340 - 14.407 µg/ml
Al	< 0.01 - 0.061 µg/ml
Fe	0.002 - 0.547 µg/ml
Na	11.855 - 55.660 µg/ml

The test apparatus for the unlimited water vapor tests was a one-gallon, stainless steel autoclave. The saturated water vapor (100% relative humidity or 100% R. H.) environment was ensured throughout the exposure by adding 150 ml of condensate water in the bottom of the autoclave. Elevated temperatures (150 or 200°C) were maintained throughout the entire test period. A data acquisition system was developed to automatically record the temperature, pressure, and relative humidity inside the autoclave at 15-minute intervals.

The specimens were prepared with a 600-grit surface finish before testing to provide a uniform and consistent surface condition. These specimens were hung in the middle of the autoclave where the temperature distribution was uniform. The galvanic effect between the stainless steel vessel and the aluminum samples was eliminated by using Telflon™ separators and aluminum hangers for the samples. Photographs of the samples were taken before and after tests.

The specimens were weighed before each test. After the initial tests, the samples were taken out of the autoclave, air dried, weighed, and then dried in a desiccator at room temperature under vacuum for about 30 minutes. This procedure ensured that any adsorbed moisture on the surface of the specimens was removed and only the weight gain due to oxidation of the aluminum was obtained. Air drying was found to provide sufficient drying and was used subsequently in the drying procedure. The weight gain data (in $\mu g/dm^2$) were obtained by normalizing the total weight gain by the sample surface area (typically, for a test coupon of 2-inch x 0.75-inch x 0.125-inch with a nominal hole of 0.125-inch diameter, the surface area is 3.712 in^2 or 0.240 dm^2). After re-weighing, the samples were put back in the autoclave for the next test interval and a fresh charge of condensate water was added (150 ml).

Surfaces and cross sections were examined by optical and scanning electron microscopy. X-ray diffraction (XRD) was used to identify the aluminum oxide film type after selected exposure conditions including water vapor alone, water with added acid, and under the radiation field. In all cases, boehmite crystals ($Al_2O_3 \cdot H_2O$) formed on the sample surfaces (Figure 1). The literature reviews state that the predominant oxide for aluminum exposed to water is boehmite at temperatures above approximately 80°C.

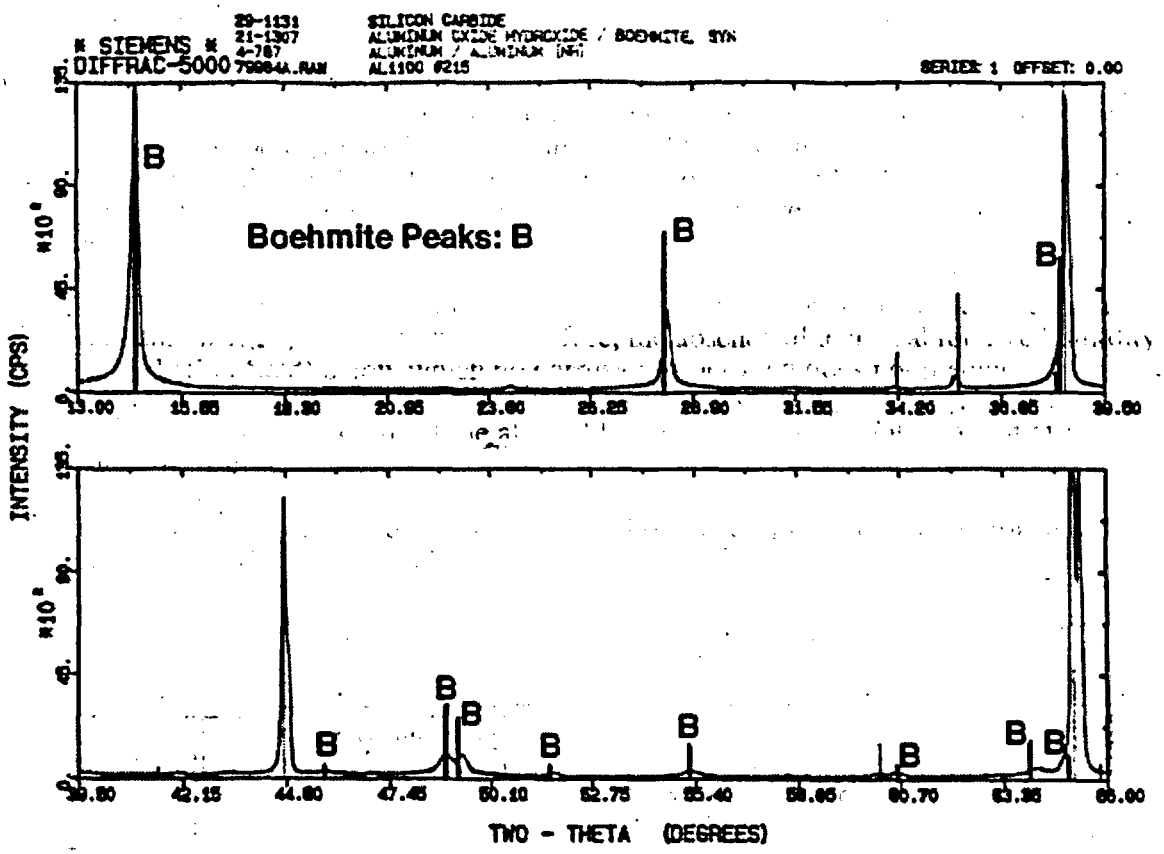

Figure 1 - Typical X-Ray Diffraction Chart with Boehmite ($Al_2O_3 \cdot H_2O$) Peaks

Results of Vapor Corrosion Tests- Aluminum Cladding Alloys, Unlimited Species

Total exposures of 1400 and 5100 hours were accumulated, respectively, for the 150°C and 200°C tests. The data points in Figures 2 to 5 show the actual weight gain results (normalized by the surface area of the specimen) while the curves represent the corrosion models using the Arrhenius relations. In general, the data for aluminum 1100 (Fig. 2) and 6061 (Fig. 3) show a parabolic corrosion behavior. Although the parabolic behavior can also be seen for 5052 initially (<1400 hours at 200°C), break-away corrosion occurred at a weight gain of about 100,000 μg/dm^2 (Figs. 4 and 5). During post-break-away behavior there is a linear relationship between the weight gain and time of exposure. Note that in Figures 4 and 5 the break-away data for 150°C were obtained by exposing the coupon samples which were previously tested at 200°C for 5100 hours. At this time the specimen has shown indications of break-away corrosion. It was assumed that the break-away is controlled by the oxide film thickness, which is directly proportional to the weight gain before the break-away corrosion takes place. Therefore, the parabolic corrosion model predicts that for a weight gain of 100,000 μg/dm^2, break-away corrosion at 150°C would occur after 16,000 hours exposure. This re-use of test coupons permits an accelerated study of break-away corrosion at a different temperature, and is valid when the same corrosion mechanism controls the process.

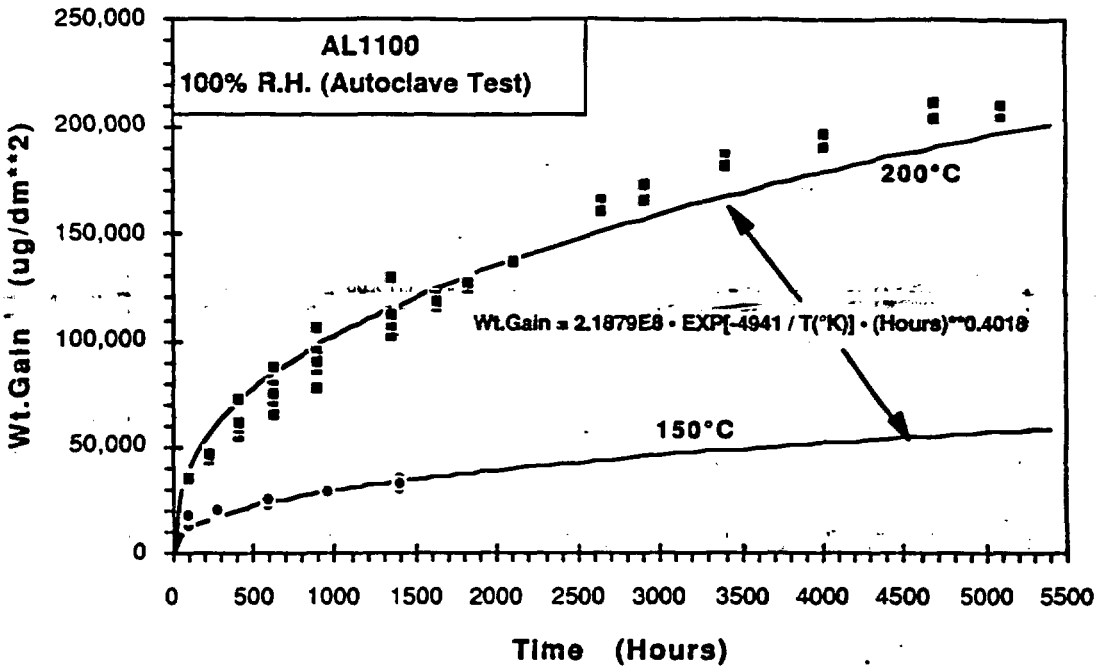

Figure 2 - Parabolic Corrosion in Aluminum 1100

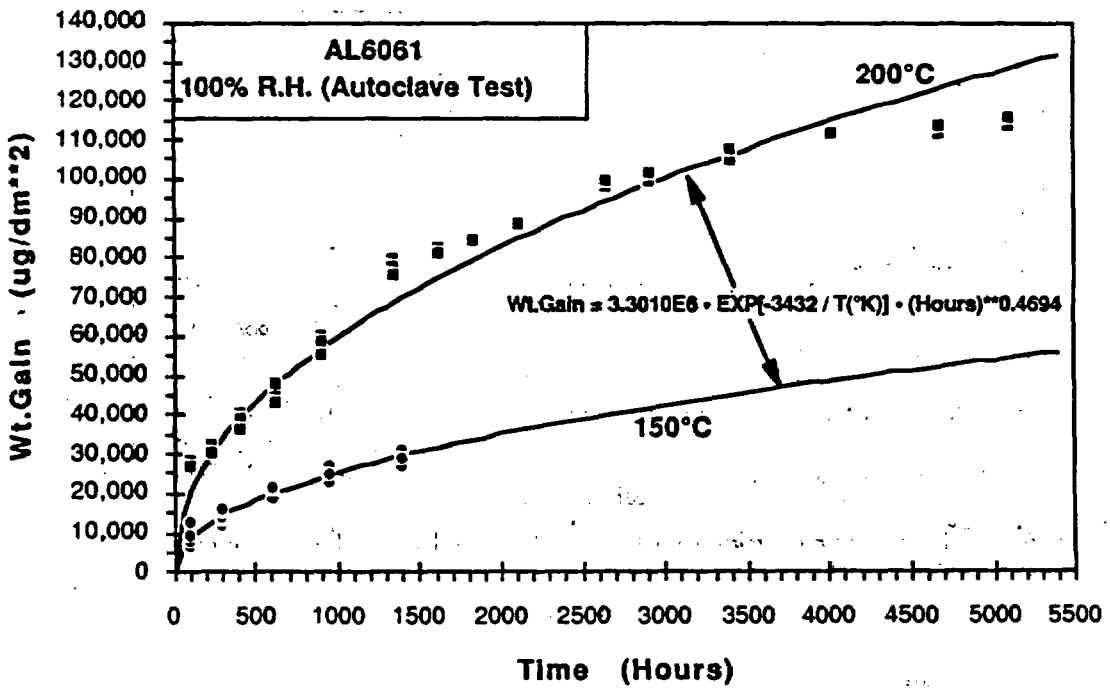

Figure 3 - Parabolic Corrosion in Aluminum 6061

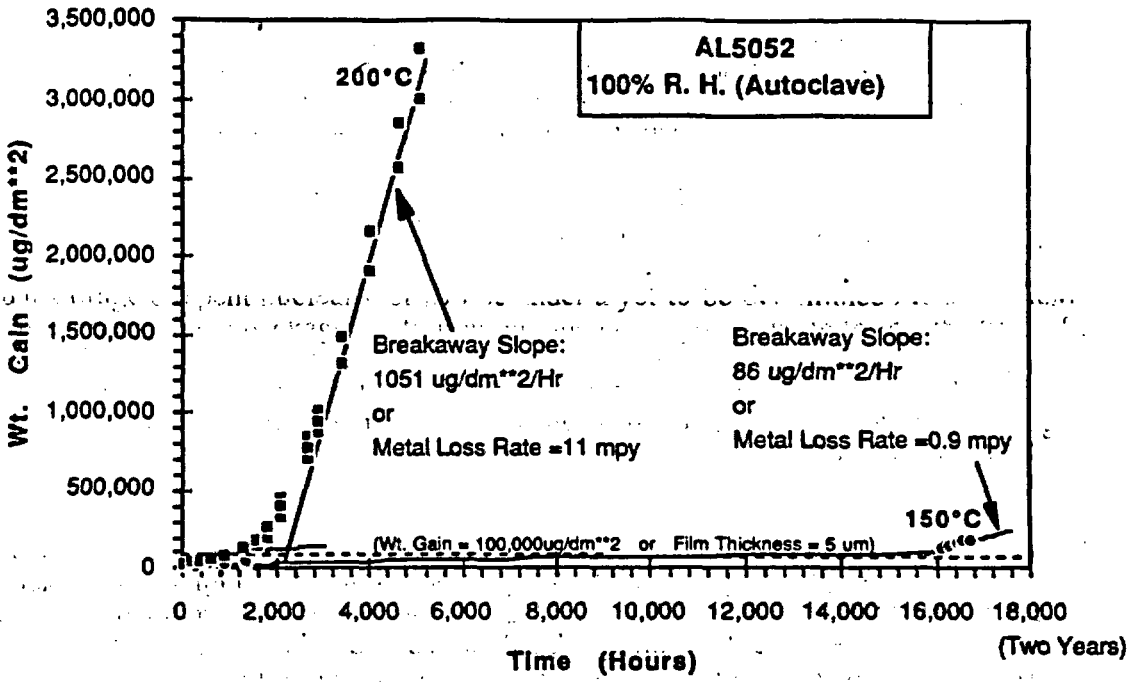

Figure 4 - Break-Away corrosion in Aluminum 5052

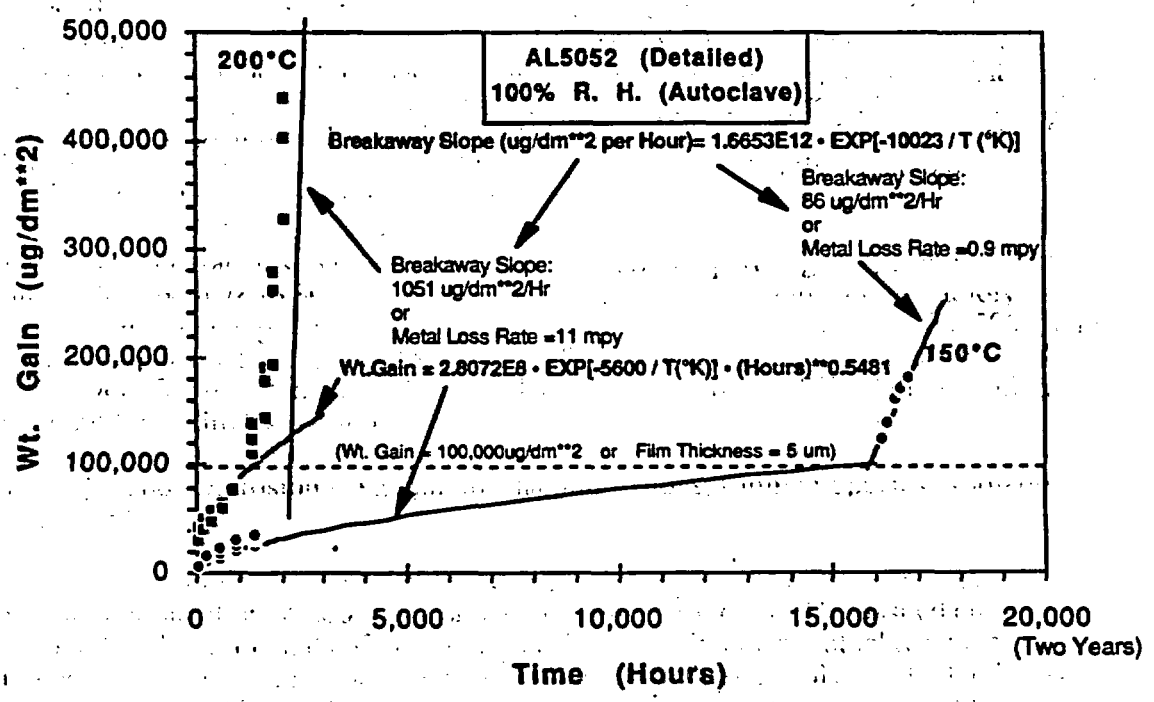

Figure 5 - Break-Away corrosion in Aluminum 5052 (Details)

All the autoclave data can be summarized in a logarithmic plot (Fig. 6). Also included in this figure is the data of Godard (1967) [ref. 1] from tests at room temperature in a saturated water vapor environment for an aluminum alloy CA-3S which is very similar to alloy 1100 in chemical composition. Note that at room temperature, bayerite or gibbsite ($Al_2O_3 \cdot 3H_2O$), rather than boehmite ($Al_2O_3 \cdot H_2O$), is more likely to form on the aluminum sample surface. Godard assumed in his paper that the oxide form was Al_2O_3 without any water of hydration.

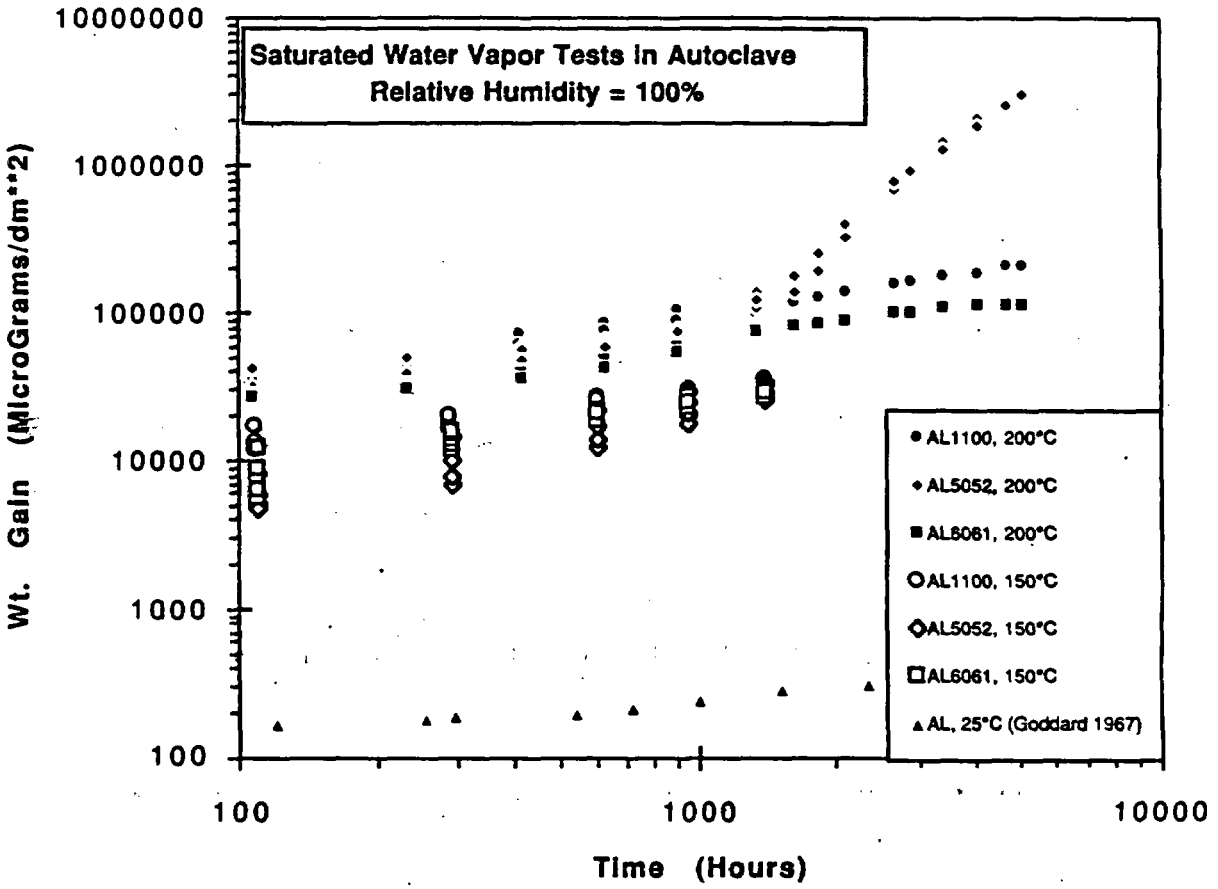

Figure 6 - Autoclave Test at 100% Relative Humidity (Saturated Water Vapor)
NOTE: Aluminum Consumed (metal loss in mils) = (1.193×10^{-6}) x Weight Gain (in $\mu g/dm^2$); Oxide Film Thickness (boehmite film in nm) = 0.053319 x Weight Gain (in $\mu g/dm^2$)

In a radioactive environment, NO_x gas will form through the radiolysis of the air. These gases will further react with water vapor and may condense on the fuel clad surface as nitric acid (HNO_3) which is an aggressive corrodant to the aluminum alloys. To simulate this radiation effect, a solution of nitric acid was added to the water condensate to achieve a pH value of 1 at room temperature in the solution mixture. The mixture was made from

one part of concentrated (15M) nitric acid and six parts of water condensate. The specimens were then tested at 150°C for one week. Very thick layers of white corrosion products were formed, and sloughing-off was observed. In this case, the weight gain data is not a reliable guide to corrosion of the aluminum. X-ray diffraction has confirmed that these oxides were boehmite. Some pitting attack of the autoclave also occurred under these conditions. After the oxide on the specimens was chemically removed, aluminum 5052 samples exhibited severe pitting corrosion, while 1100 and 6061 showed general corrosion. The metal loss data, in terms of thickness in mils, were plotted in Figure 7. Also plotted in this figure is the metal loss curves with water vapor only (converted from the weight gain curves in Figures 2 to 4). In the case of aluminum 5052, the conversion was based on general corrosion attack despite the fact that pitting had occurred. It is noted that the corrosion in an acidic water vapor environment is about two orders of magnitude higher than in an environment of water vapor only. This implies that radiolysis could have caused a significant increase in corrosion, especially at elevated temperatures.

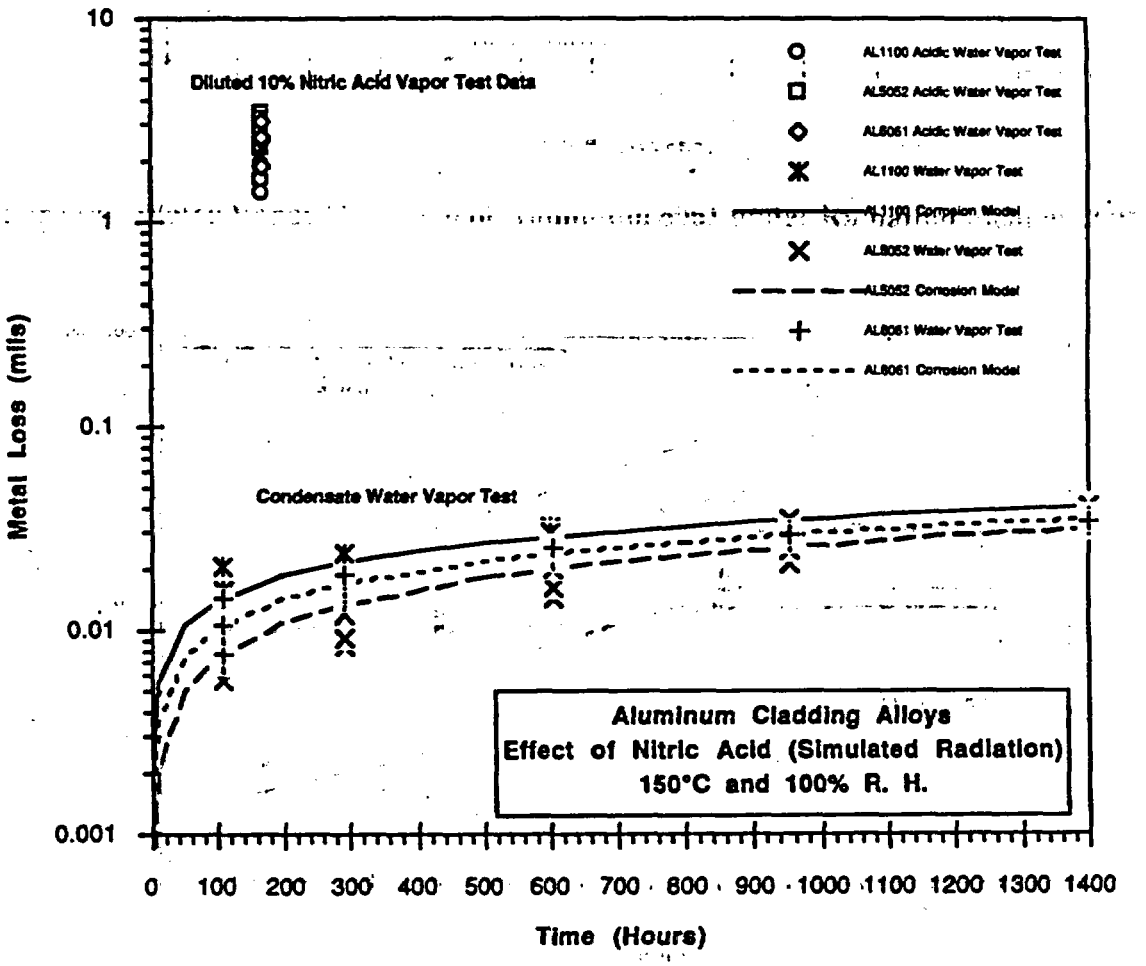

Figure 7 - Metal Loss in a Saturated Acidic Water Vapor Environment at 150°C

Post-Exposure Surface Oxide Morphology
(High Temperature Water Vapor Exposure)

Scanning electron microscopy (SEM) was performed on selected specimens after exposure to the 200°C water vapor environment. Figure 8(a)† shows a typical boehmite crystal formation (500X) on the surface of an aluminum specimen after testing. At a magnification factor of 1000X, the boehmite crystals are shown in Figure 8(b). These photographs show that the boehmite crystals grew uniformly on the sample surfaces.

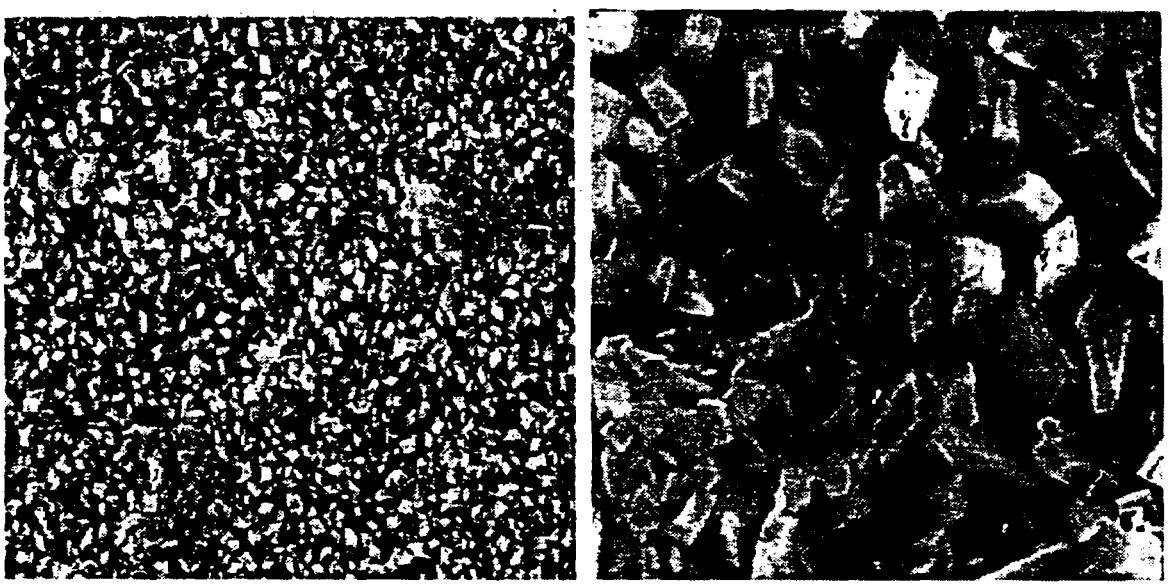

(a) Aluminum 6061 Surface (2000X) (b) Aluminum 6061 Surface (10,000X)

Figure 8 - Boehmite Crystals Formed On Aluminum Alloy Surface

Vapor Corrosion Models

The oxide growth rate for general corrosion is proportional to concentration gradient of the oxidizing species within the oxide film. It can be shown that a power law follows:

$$W = C\, t^n,$$

where W is the weight gain (or the oxide film thickness which is proportional to the weight gain, if internal oxidation does not occur), t is the exposure time, n is an exponent (n= 0.5 for a pure parabolic model), and C is related to the mobility of the diffusing species. An Arrhenius relation is used to describe the temperature dependence of the weight gain. Therefore,

† Figures 8(a,b) were obtained at the University of South Carolina at Columbia by Professor Anthony P. Reynolds in the Department of Mechanical Engineering under SCUREF (South Carolina Universities Research and Education Foundation) Task No. 212.

$$W = A \cdot \exp(-Q_1/RT) \cdot t^n,$$

where A is a coefficient which, in general, is a function of material, relative humidity, corrodant species, etc., Q_1 is related to the diffusion of oxygen in the oxide film or activation energy of boehmite, R is the universal gas constant (R= 8.31434 J/g•mole•K or R= 1.98717 cal/mole) and T is the absolute temperature in Kelvin.

In the break-away corrosion regime, it is also assumed that an Arrhenius relation exists for the weight gain (W') (the straight line portion of the weight gain in Figure 4). Note that in this regime, the weight gain is no longer proportional to the oxide film thickness , but it is still proportional to the metal loss (metal consumption). The Arrhenius relation for the weight gain in the break-away regime is

$$W' = B_o + B \cdot \exp(-Q_2/RT) \cdot t \text{ , where}$$

where B and B_o are coefficients which may be functions of material, relative humidity, corrodant species, etc., and Q_2 may be related to the diffusion of oxygen through the crystal lattice or along microstructural paths.

With the above general models, a curve fitting algorithm was developed using weight gain data from tests at temperatures of 150 and 200°C. The weight gain equations (for corrosion in saturated water vapor environments) for each of the aluminum alloys are:

- Alloy 1100:
  Wt. Gain (in $\mu g/dm^2$) = $2.19 \times 10^8 \cdot \exp[-9.82(kcal/mole)/RT(K)] \cdot (Hours)^{0.40}$
- Alloy 5052:
  - (1) Before break-away corrosion
    Wt. Gain (in $\mu g/dm^2$) = $2.81 \times 10^8 \cdot \exp[-11.13(kcal/mole)/RT(K)] \cdot (Hours)^{0.55}$
  - (2) Post-Breakaway
    Rate of Weight Gain ($\mu g/dm^2$ per Hour)= $1.67 \times 10^{12} \cdot \exp[-19.92(kcal/mole)/RT(K)]$
- Alloy 6061:
  Wt. Gain (in $\mu g/dm^2$) = $3.30 \times 10^6 \cdot \exp[-6.82(kcal/mole)/RT(K)] \cdot (Hours)^{0.47}$

The coefficients for the Arrhenius power law corrosion model with respect to each of the aluminum alloys are also tabulated in Table 4:

Table 4 - Coefficients for Arrhenius Power Law Corrosion Model

Aluminum Alloy Type	Corrosion Model: $W = A \cdot \exp(-Q_1/RT) \cdot t^n$		
	A: $(\mu g/dm^2)/Hour^n$	Q_1: kcal/mole	n
1100	2.19×10^8	9.82	0.40
5052 (Pre-Breakaway)	2.81×10^8	11.13	0.55
6061	3.30×10^6	6.82	0.47

Note: The model is based on test data obtained at 150 and 200°C in saturated vapor environments.
W: Weight Gain per Unit Surface Area ($\mu g/dm^2$)
R: Universal Gas Constant (1.98717 cal/mole)
T: Absolute Temperature (degrees Kelvin)
t: Time in Hours

Based on the corrosion of aluminum to form boehmite,

$$2\ Al + 4\ H_2O \text{ ---> } Al_2O_3 \cdot H_2O + 3\ H_2$$

the following conversion formulae in terms of weight gain value can be derived:

- Aluminum Consumed (or Metal Loss in mils) = (1.19×10^{-6}) x Weight Gain (in $\mu g/dm^2$)
  ------ Valid for both pre- and post break-away corrosion;
- Oxide Film Thickness (Boehmite Film in nm) = (5.33×10^{-2}) x Weight Gain (in $\mu g/dm^2$)
  ------ Valid only prior to break-away corrosion,

in which the aluminum alloy density of 2.7 g/cc and the boehmite density of 3.41 g/cc were used.

An experiment was set up to validate the weight gain to oxide film thickness conversion in the parabolic regime. Three specimens (aluminum 1100 #047, aluminum 5052 #073, and aluminum 6061 #093 after an exposure to water vapor for 1348 hours) were sectioned, mounted, ground, and polished to reveal the oxide layers. Five 500X photographs were taken at randomly selected locations for each alloy specimen cross-section. For each photograph, five random measurements were taken for the oxide film thickness. A total of 25 measurements were obtained for each specimen. As shown in Table 5., the averaged values agree very well with the calculated oxide film thicknesses based on the weight gain data:

Table 5 - Oxide Layer Thickness

Alloy Type	Weight Gain	Oxide Layer Thickness	
(1348 hours in 200°C Water Vapor)	($\mu g/dm^2$)	Measured & Averaged (μm)	Calculated (μm)
1100	112,000	6.07	5.97
5052	122,000	6.16	6.50
6061	80,000	4.42	4.26

4.0 VAPOR CORROSION OF ALUMINUM CLADDING ALLOYS - LIMITED CORRODANT (NO RADIATION)

An autoclave was used for the 100% relative humidity water vapor test. In principal, the autoclave can also be used for tests other than 100% relative humidity by calculating the amount of water condensate that is needed. However, the amount of water vapor that may condense on the cooler parts of the autoclave is uncertain, and the relative humidity cannot be accurately controlled. In addition, long term tests with nitric acid to simulate radiation would cause damage to the stainless steel autoclave. Therefore, specially designed, stainless steel capsules for one test use were placed in furnaces for both the water vapor and acidic water vapor tests. Under these conditions, corrosion stops when the corrodant species, such as water and oxygen, are consumed by the oxidation process, as long as the encapsulating system remains intact.

Figure 9 shows the configuration of the test capsules. The capsules were made of two 1.5-inch Schedule 10 stainless steel pipe caps (outside diameter is 1.9 inches) with a

volume of about 78 ml. The two pipe caps were joined by electron beam welding a machined rabbit joint. A fill tube (1/8-inch diameter) on the upper pipe cap was gas tungsten arc welded to the capsule. The capsule could hold several coupon specimens. Typically, the capsules contained one of each type aluminum alloy (1100, 5052, and 6061). Water was added to the capsule through the fill tube and then the tube was sealed by welding. The water vapor saturation pressures at the intended test temperature of 150, 200, and 250°C are, respectively, 69, 226, and 577 psia. Therefore, the capsules were pressure checked and helium leak checked prior to use.

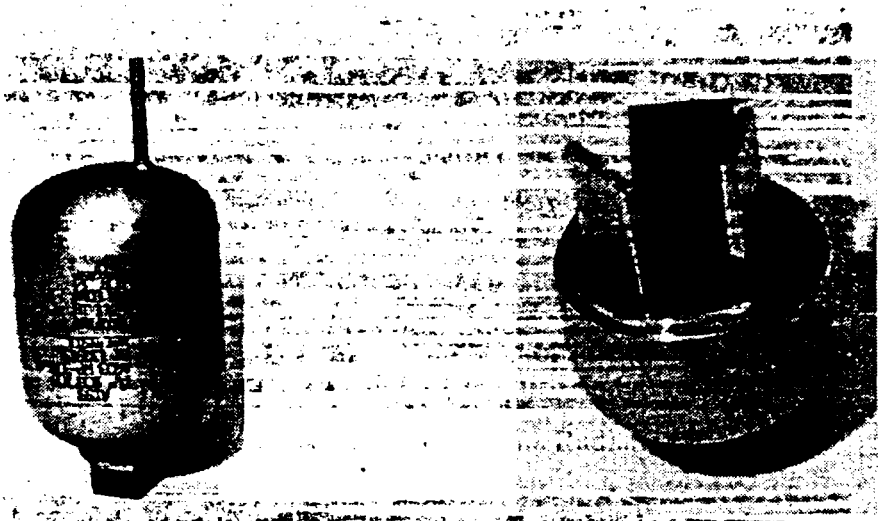

(a) Capsule is Made of Two Pipe Caps (b) Three Coupon Specimens are Installed

Figure 9 - Stainless Steel Capsule for Corrosion Test

The amount of water condensate (V_{water}) to be injected into the sample-containing capsule to provide a target initial relative humidity condition at the test temperature is calculated as

$$V_{water} = (V_{capsule} - V_{samples})/(\rho_{water} \cdot V_s),$$

where $V_{capsule}$ is the volume of the capsule, $V_{samples}$ is the total volume of the specimens, ρ_{water} is the density of the water condensate (normally, 1 g/cc is used), V_s is the specific volume of the water condensate and is a function of test temperature and the vapor pressure (P) corresponding to the desired initial relative humidity (RH) of the capsule. The values of specific volume are tabulated in steam tables. For the selected relative humidity, the corresponding vapor pressure for the test temperature is

$P = P_{sat} \cdot RH$, where P_{sat} is the saturation vapor pressure also given in the steam tables.

Similar to the nitric acid vapor test in the autoclave, a nitric acid solution with initial pH about 1 was prepared for the capsule test. The mixture was made from one part of concentrated (15M) nitric acid and six parts of water condensate. In estimating the amount of solution mixture to be injected into the test capsule with an assigned initial relative humidity, three water sources are considered: 1) water contained in the

concentrated (15M) acid, 2) water used to dilute the concentrated (15M) acid, and 3) water dissociated from nitric acid at high temperature, that is

$$4\ HNO_3 \text{ ---> } 4\ NO_2 + O_2 + 2\ H_2O \text{ (at elevated temperature)}$$

Therefore, the amount of the diluted solution mixture (V_{mix}) to be injected to a capsule with a designated relative humidity can be calculated as

$$V_{mix} = [(V_{capsule} - V_{samples})/V_s] /[\ (1 - \alpha_v) \cdot \rho_{water} + \alpha_v \cdot \rho_{stock} \cdot (1 - \alpha_w + \beta \cdot \alpha_w)\ ],$$

where ρ_{stock} is the density of the concentrated (15M) acid;

α_w is the weight percent of the acid, normally labeled on the concentrated (15M) acid bottle;

α_v is the volume percent of the concentrated (15M) acid in the diluted mixture (i.e., α_v = (number of parts of the concentrated (15M) acid) / (number of parts of water condensate + number of parts of concentrated (15M) acid); and

β is the ratio of the weight of water to the weight of nitric acid in the HNO_3 dissociation equation above, or

$$\beta = (2 \cdot \text{molecular weight of } H_2O) /(4 \cdot \text{molecular weight of } HNO_3).$$

In addition to the individual specimen weights, the total weight of capsule, water, and test specimens was recorded. The total weight was measured to check for a loss in weight which would indicate water loss through capsule failure during the test. The capsules were put in ovens and were taken out according to the assigned test duration. The capsules were then cut open and the samples inside the capsules were weighed.

Results of Vapor Corrosion Tests - Aluminum Cladding Alloys: Limited Species

Figures 10 to 12 respectively summarize the capsule test data for aluminum 1100, 6061, and 5052 at 150°C for 12 months. Note that the relative humidity values labeled in these figures are their initial values. As the exposure time increases, the relative humidity decreases due to the consumption of water in the corrosion process. The following conclusions can be drawn:

(1) Vapor from the nitric acid solution, or the simulated radiolysis environment, has significantly increased corrosion.

(2) Corrosion is more extensive in an environment with higher relative humidity.

(3) The corrosion rate will decrease and will eventually cease. The capsule is a completely closed system. The amount of air, water, and/or acid is fixed as soon as the capsules were sealed; the corrodant species were depleted due to the oxidation reaction ($2\ Al + 4\ H_2O$ ---> $Al_2O_3 \cdot H_2O + 3\ H_2$).

(4) Under a water vapor environment, a critical relative humidity between 40 to 70% exists below which practically no corrosion occurs at room temperature (Vernon 1931, [ref. 2]). It appears that in the current capsule test, the critical relative humidity

at 150°C is 20% for 1100 and 6061 because no distinct weight gain was observed after exposures up to 9000 hours.

(5) Based on the present data, the critical relative humidity for alloy 5052 under a water vapor environment at 150°C is less than 20%. All three aluminum alloys (1100, 5052, 6061) exhibited weight gains in the acidic or simulated radiation environment at 20% relative humidity; therefore, a threshold water level below which corrosion does not occur was not observed.

(6) In a closed system, the corrosion will stop when all the corrodant species (e.g., free water and oxygen) are consumed; therefore, the absence of a critical relative humidity (in a radiation field) below which no corrosion is detected does not preclude acceptable fuel storage in a completely sealed containment system as long as the acceptance criteria in terms of the allowable corrosion or allowable amount of free water are specified.

(7) At the end of test, the residual relative humidity, vapor pressure, and hydrogen generation can be calculated based on the weight gain data.

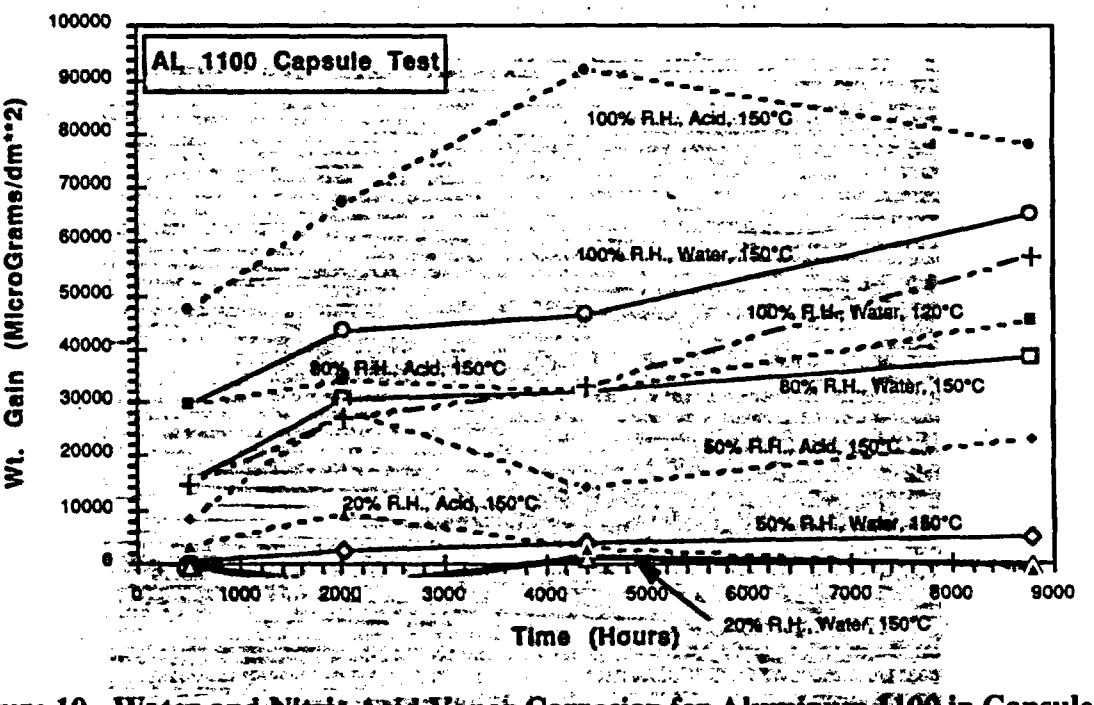

Figure 10 - Water and Nitric Acid Vapor Corrosion for Aluminum 1100 in Capsules

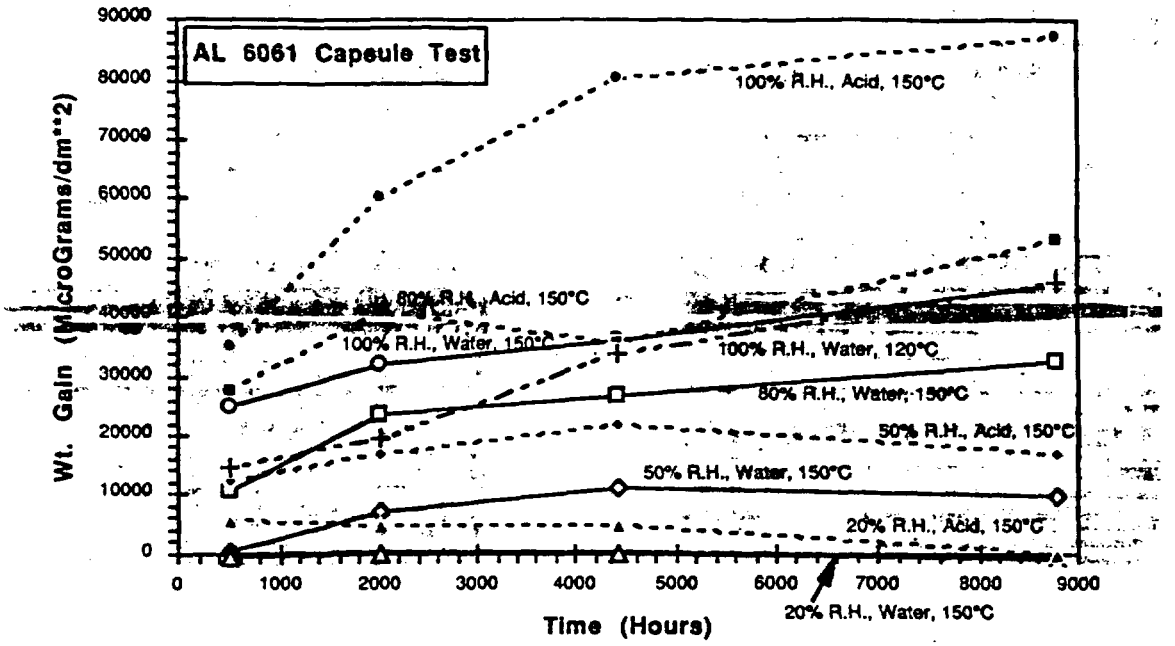

Figure 11 - Water and Nitric Acid Vapor Corrosion for Aluminum 6061 in Capsules

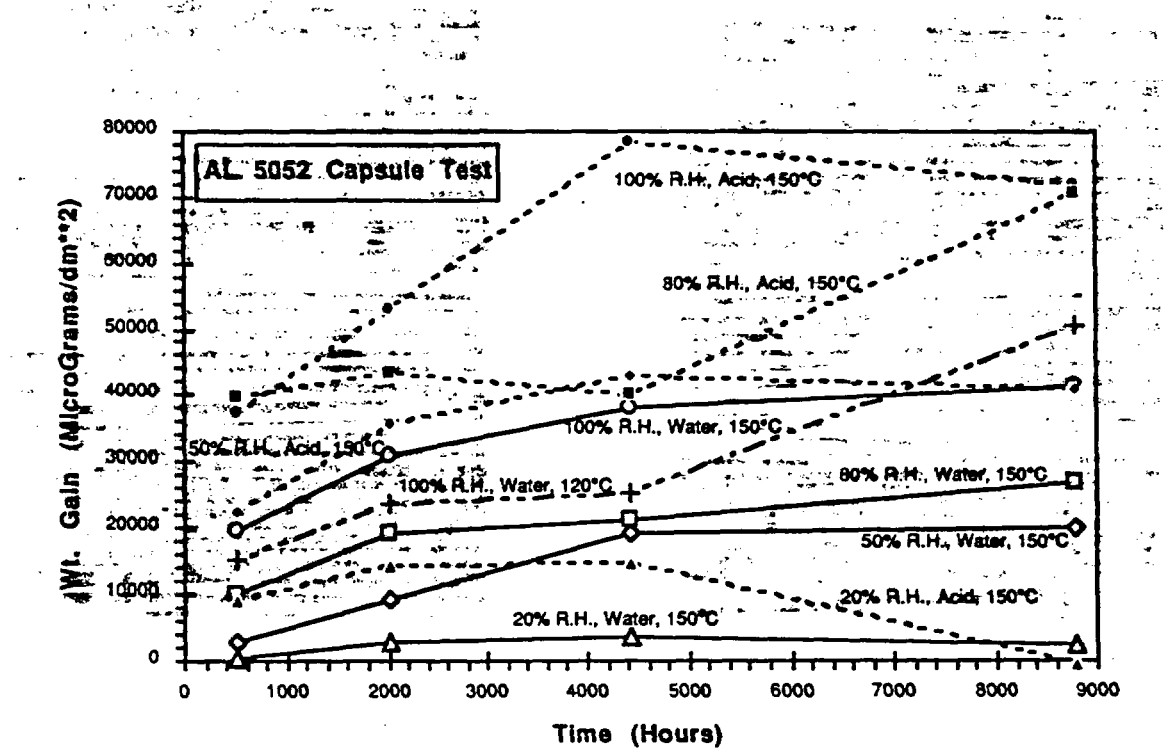

Figure 12 - Water and Nitric Acid Vapor Corrosion for Aluminum 5052 in Capsules

A verification test was run at 120°C in a separate oven. Four capsules were prepared with 100% R. H water condensate and were taken out for weight gain measurement at the same time intervals as the 150°C capsules (3 weeks, 3, 6, and 12 months). It was demonstrated that the weight gain curve of 120°C is indeed below that obtained at a 100% relative humidity with a higher temperature, 150°C.

5.0 VAPOR CORROSION OF ALUMINUM CLADDING ALLOYS - LIMITED CORRODANT UNDER GAMMA RADIATION

Actual storage of spent nuclear fuel will be under a yet-to-be-determined radiation field which depends on the package configurations and co-disposed waste forms, the type of fuel, fuel burn-up, and decay times. As has been demonstrated (nitric acid water vapor environments), the corrosion rates were significantly increased in the tests under the simulated radiation environment. To investigate corrosion behavior under an ionizing radiation field, the test capsules described in section 4 were loaded for exposure in the SRTC gamma cell facility.

A rack to hold six capsules was designed. A heating element was placed in the center of the rack. The assembly was put inside a can which is insulated and provides more uniform temperature distribution for the capsules. Building air was introduced to the exterior of the can for cooling purpose so that the gamma cell chamber would maintain a safe operating temperature (below 100°C). Two thermocouple lead wires, an electric cord for the heating element, and an air tube were fed through the limited opening leading to the test chamber.

The capsules, each containing an 1100, a 5052, and a 6061 specimen, were filled with water condensate to produce initial relative humidities of 20, 50, and 100%. These capsules were tested at 200°C for 1, 4, 8, and 12 weeks. A thermocouple was attached to a capsule to confirm the test temperature and a separate thermocouple was mounted on the outside of the can (which enclosed the rack and capsules) to prevent overheating the gamma cell. The gamma cell contains a cobalt 60 source and has a fixed dose rate of 1,810,000 R/hr (current value). Note that this intensity is higher than that expected during spent nuclear fuel storage in the repository.

In addition, a separate test was carried out at the normal operating temperature of the gamma cell - about 78 to 80°C. This test investigated the low temperature radiolysis effect in a saturated vapor environment. Two capsules, each containing 1100, 5052, and 6061 test coupons, were exposed for periods of one and four weeks, respectively. These capsules were filled with excess water condensate to maintain 100% relative humidity throughout the entire test period.

Results of Vapor Corrosion - Aluminum Cladding Alloys, Limited Species, Radiation Environment

The results for aluminum 1100, 6061, and 5052 under the condition of air/water vapor/gamma radiation at 200°C are shown in Figures 13 to 15. The dashed curves correspond to the test results of unlimited species corrosion in an autoclave under saturated water vapor condition and were inserted for reference only. Note that in Figure 15 for aluminum 5052, the dashed curve is valid up to a weight gain about 100,000 $\mu g/dm^2$, beyond which the break-away corrosion occurred. It is seen that in the case of

initial 100% relative humidity, the radiolysis effects in the water/air environment caused a weight gain about three times as great from that in the water/air environment without radiation in the early stage of the corrosion. After a very short period of time, less than a week, most of the corrosion has occurred and either the usable water vapor corrodant has been depleted or the oxide film has reached a thickness sufficient to significantly decrease the corrosion rate. This is indicated by the flattening of the weight gain curves (of the capsule test in gamma cell). Figures 13 to 15 also include data points for "zero" relative humidity in which case the capsules were loaded with test coupons at ambient room conditions. A small weight gain was observed. The 20% relative humidity data for aluminum 1100 (Fig. 13) showed an abnormal trend. It is not clear what caused this trend.

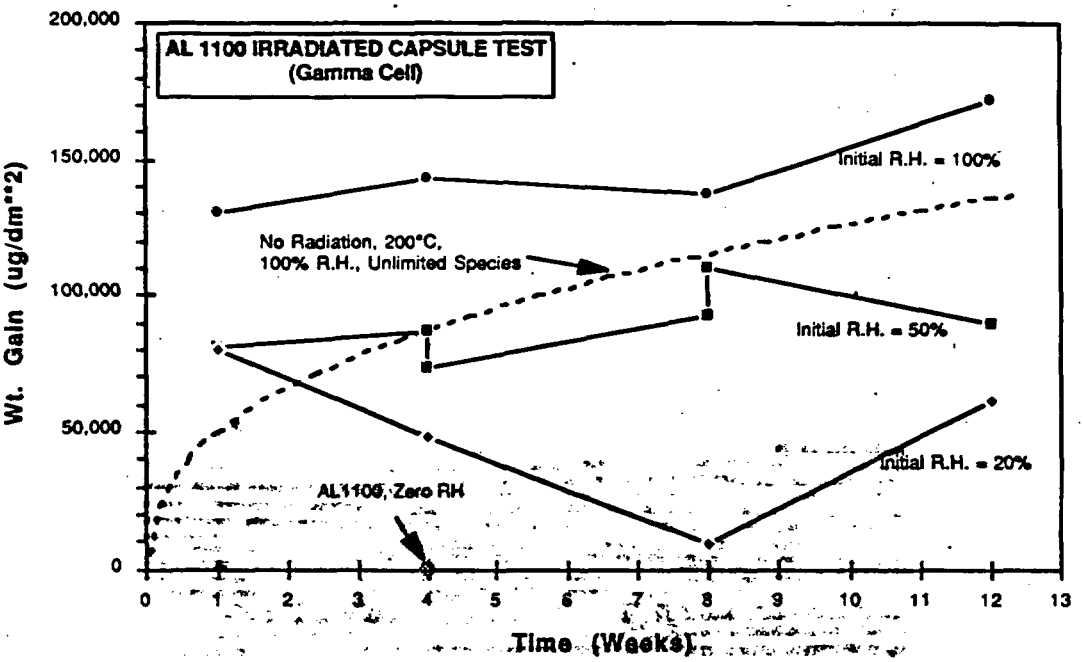

Figure 13 - Water Vapor Corrosion of Aluminum 1100 under Radiation Field at 200°C

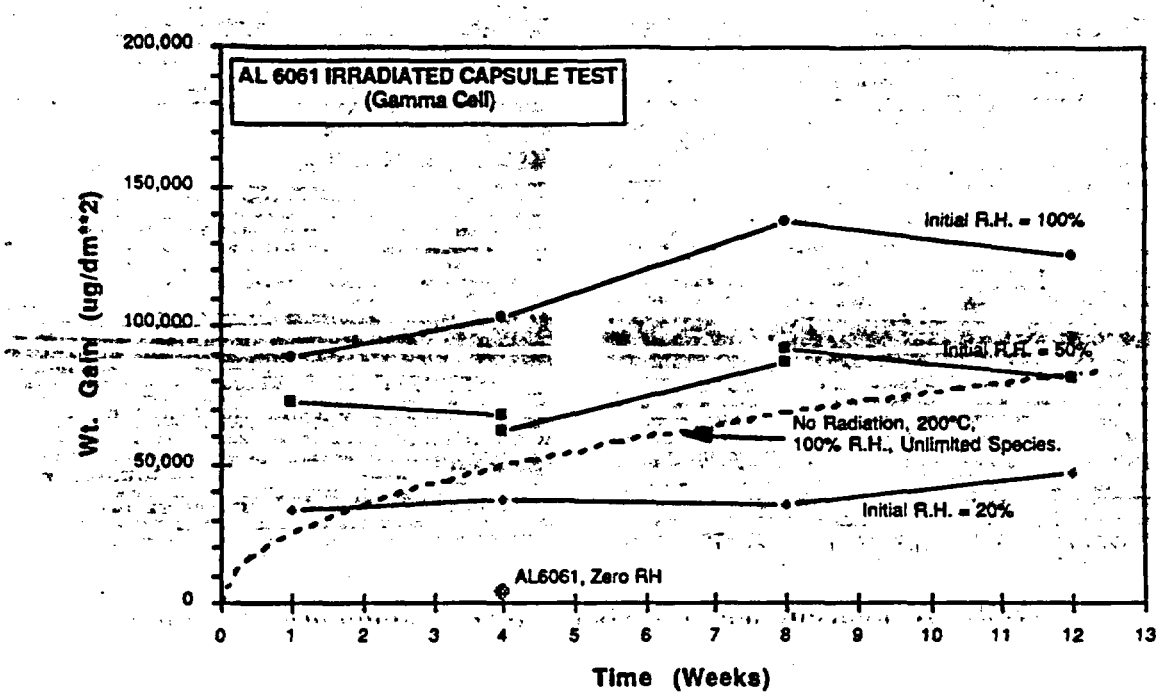

Figure 14 - Water Vapor Corrosion of Aluminum 6061 under Radiation Field at 200°C

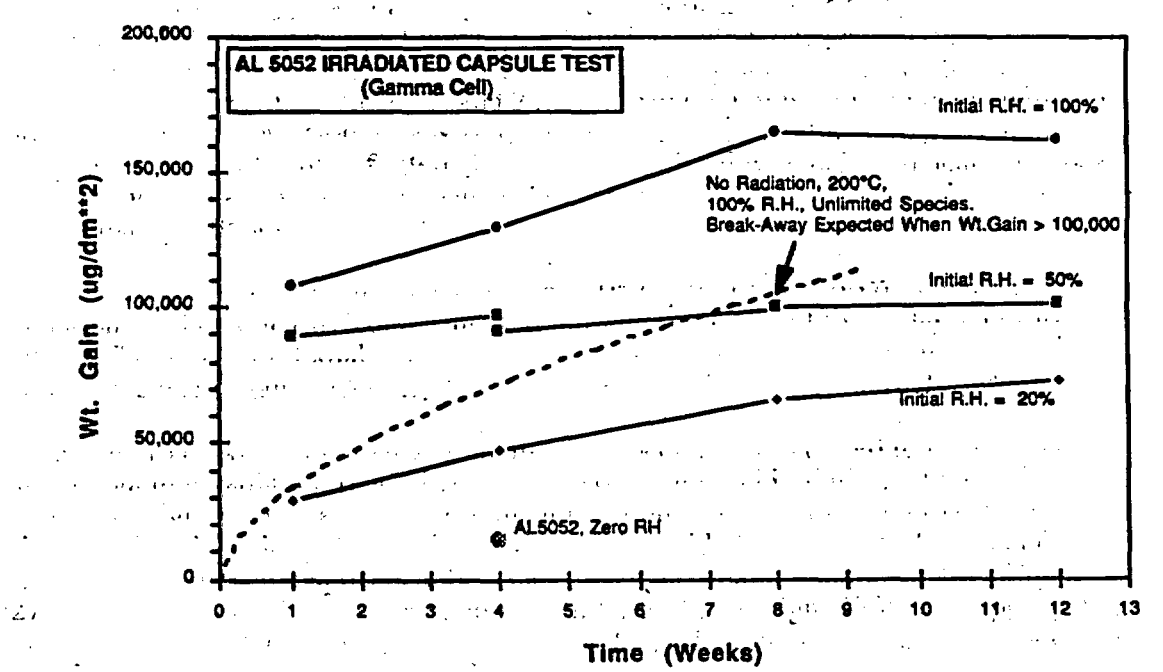

Figure 15 - Water Vapor Corrosion of Aluminum 5052 under Radiation Field at 200°C

The radiolysis effects at lower temperature are also of interest. The spent fuel is not expected to be constantly subject to the specified upper temperature limit of the repository. A capsule test was carried out at the normal operating temperature of the gamma cell, 78 to 80°C. Two data points were obtained after exposures of one and four weeks, respectively. These capsules were filled with a sufficient amount of water to maintain a constant 100% relative humidity throughout the test periods. The data points (filled circles) for aluminum 1100, 6061, and 5052 are shown in Figures 16 to 18. These figures also include: 1) a reference set of unlimited species test data (autoclave result) at 150°C and its fitted curve (see Section 3.0 or the Arrhenius equations shown in Figures 2, 3 ,and 5); 2) a set of data obtained by Godard (1967) for CA-3S aluminum which is similar to aluminum 1100; and 3) predicted corrosion responses at 78 and 25°C based on the Arrhenius equations for aluminum 1100. It can be seen that the aluminum 1100 prediction curve at 25°C closely represents Godard's CA-3S data. In contrast, the weight gain data for the 78°C test are comparable to the 150°C data without radiation and are at least 5 times the predictive values at the end of the 4-week test at 78°C. It should be noted that Godard's CA-3 aluminum is not equivalent to aluminum 5052 and 6061, but the data were included in Figures 17 and 18 for reference only. It is therefore not unexpected that the 25°C prediction curves (based on aluminum 1100) in these two figures disagree with the Godard's data. It is also possible that the extrapolation of the Arrhenius equation may yield unusual results.

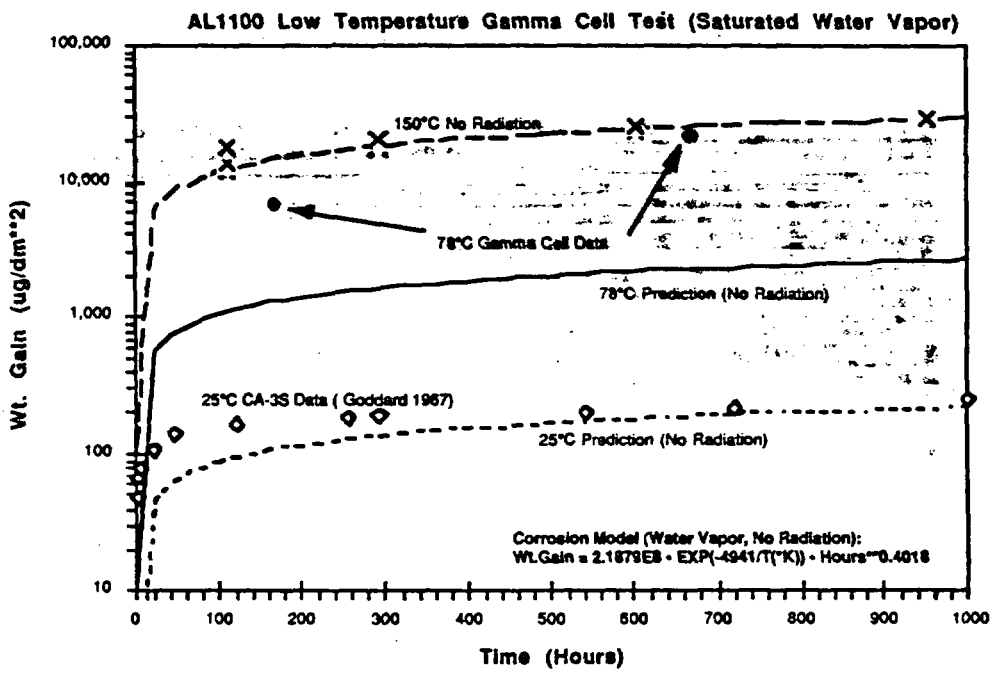

Figure 16 - Effects of Water Vapor Corrosion under Radiation Field at 78°C Aluminum 1100)

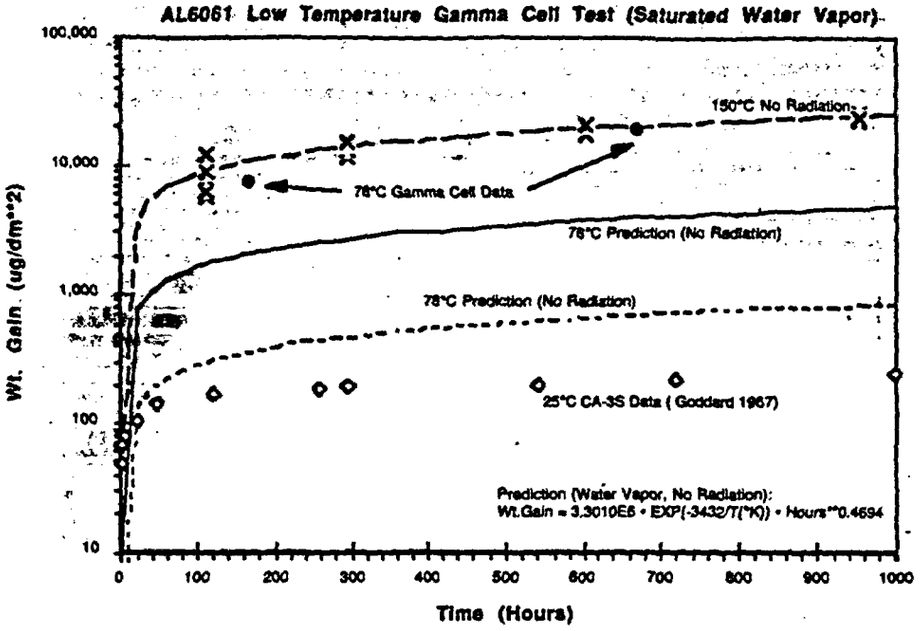

Figure 17 - Effects of Water Vapor Corrosion under Radiation Field at 78°C (Aluminum 6061)

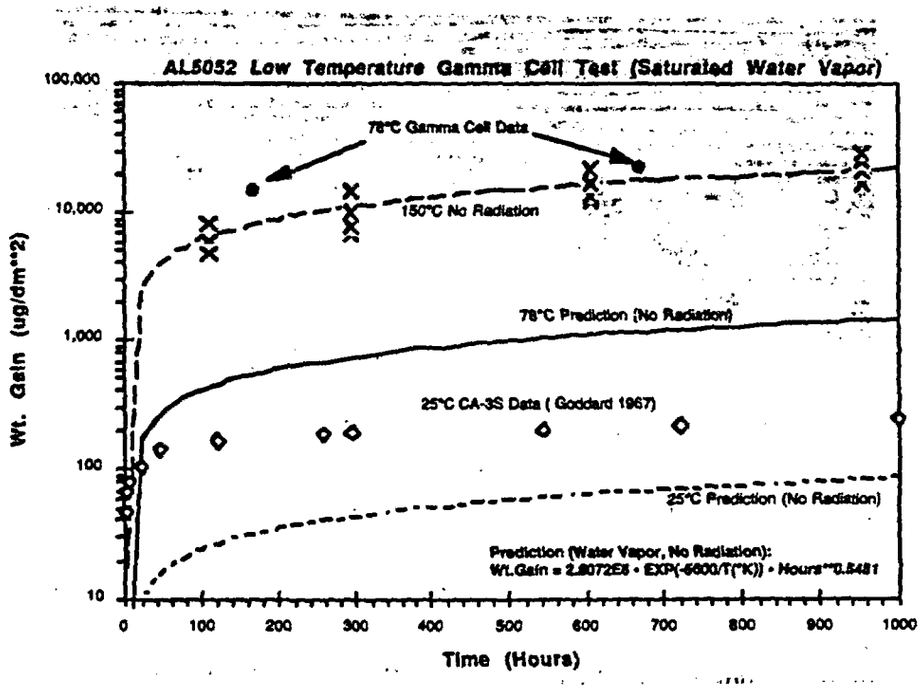

Figure 18 - Effects of Water Vapor Corrosion under Radiation Field at 78°C (Aluminum 5052)

The test showed that the corrosion of aluminum 5052 was greater than that of aluminum 1100 and 6061. The full impact due to radiation is yet to be assessed (e.g., microstructural examination of 5052 in cross-section) because internal oxidation is known now to exist in 5052 alloy in high temperature tests (Section 6.0).

It is clear from the test data that a threshold for relative humidity does not exist in a substantial gamma radiation field. A noticeable amount of corrosion has occurred at 20% relative humidity. However, in this test with a high dose rate, the water vapor corrodant is consumed quickly in the first week and the corrosion rate is then significantly reduced.

Post-Exposure Surface Oxide Morphology
(Under High Temperature Water Vapor/Gamma Radiation Conditions)

The surfaces of the test coupons were examined by SEM for all 100% relative humidity specimens. Compared to the specimens exposed to water vapor only (Fig. 8), a completely different oxide morphology was formed in the presence of a gamma radiation field. The SEM photographs of one week and twelve-week exposures under 1.81×10^6 R/hr are shown in Figures 19 to 21 for all three aluminum alloys. High magnification examinations of a typical specimen surface after only one-week exposure are shown in Figure 22 (aluminum 6061 is used for illustrative purpose). It can be seen that the oxide surface is no longer evenly paved by boehmite crystals with similar sizes (as in Figure 8). The flatter surfaces are still covered by fine crystals (Figure 22(d)). Variable sizes of crystal clusters can be seen in Figures 22(b) and 22(c), along with crater-like opened blisters. Some blisters appeared intact, especially in the one-week specimens. As the exposure time increases, more blisters appeared to be cracked. Some open blisters show the underlying crystalline structure, believed to be boehmite as determined by XRD (Fig. 1).

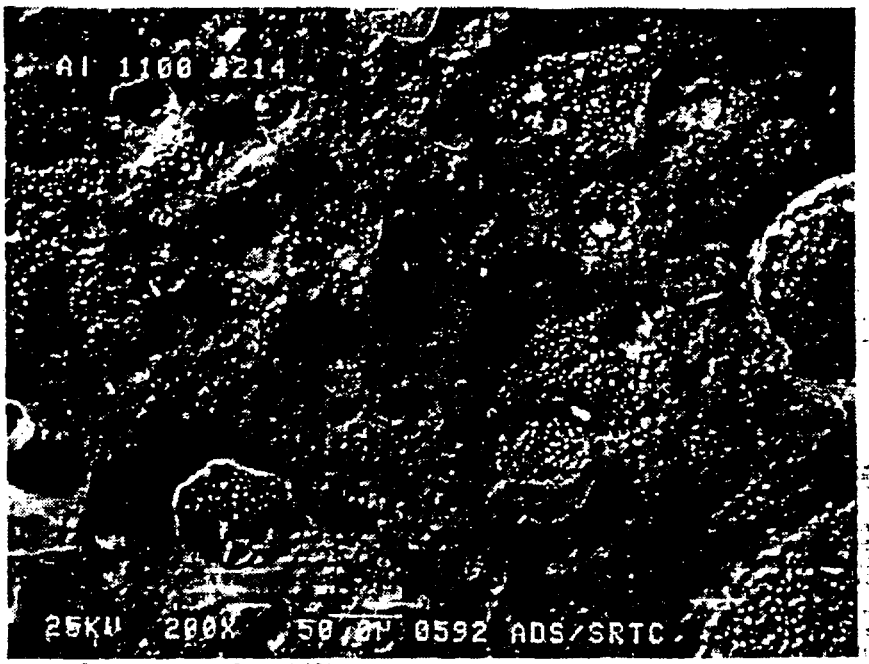

(a) 1 Week of Exposure in Gamma Radiation Field

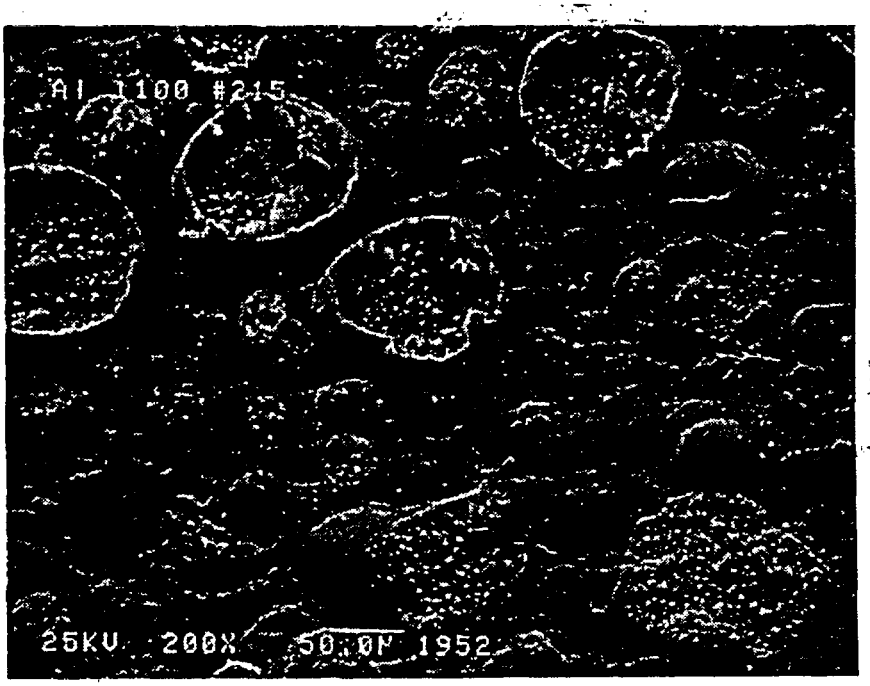

(b) 12 Weeks of Exposure in Gamma Radiation Field

Figure 19 - Aluminum 1100 in Saturated Water Vapor at 200°C Exposed to Gamma Radiation Field

(a) 1 Week of Exposure in Gamma Radiation Field

(a) 12 Week of Exposure in Gamma Radiation Field

Figure 20- Aluminum 6061 in Saturated Water Vapor at 200°C Exposed to Gamma Radiation Field

(a) 1 Week of Exposure in Gamma Radiation Field

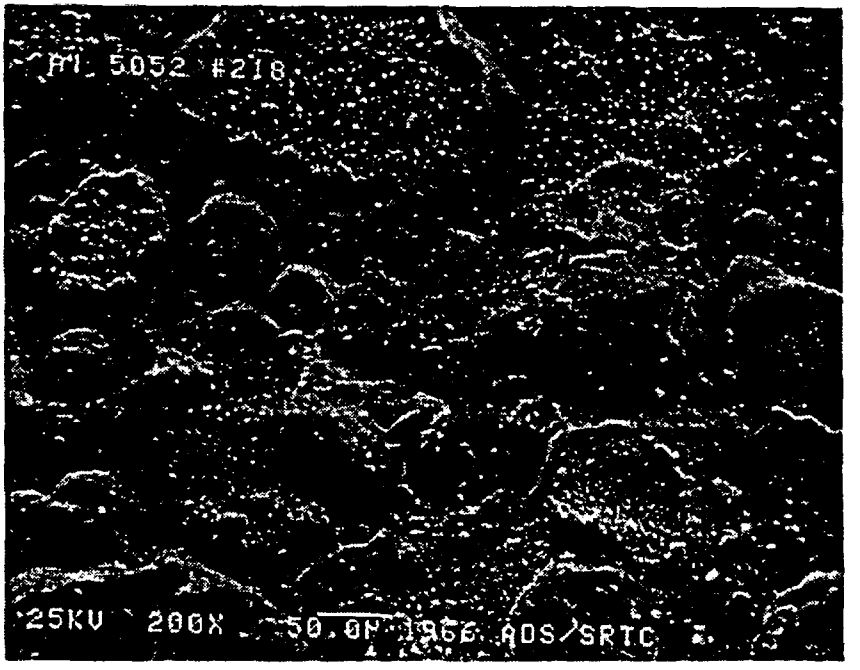

(b) 12 Week of Exposure in Gamma Radiation Field

Figure 21 - Aluminum 5052 in Saturated Water Vapor at 200°C Exposed to Gamma Radiation Field

(a) 500X

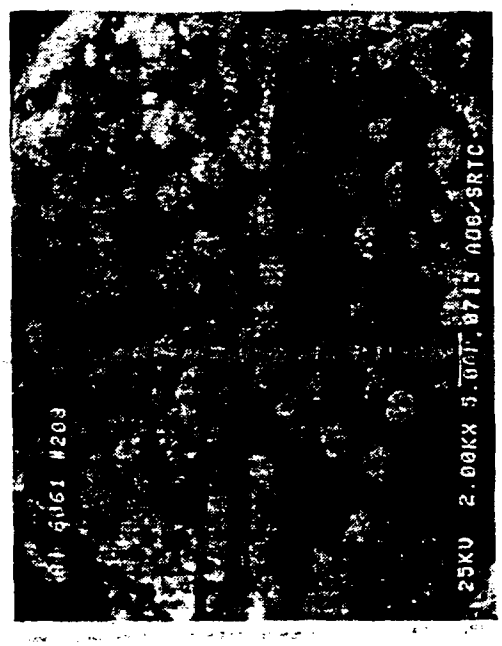

(b) 2000X

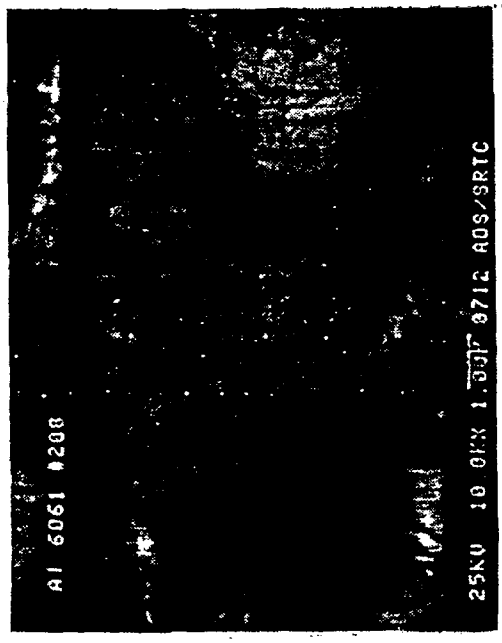

(c) 10,000X

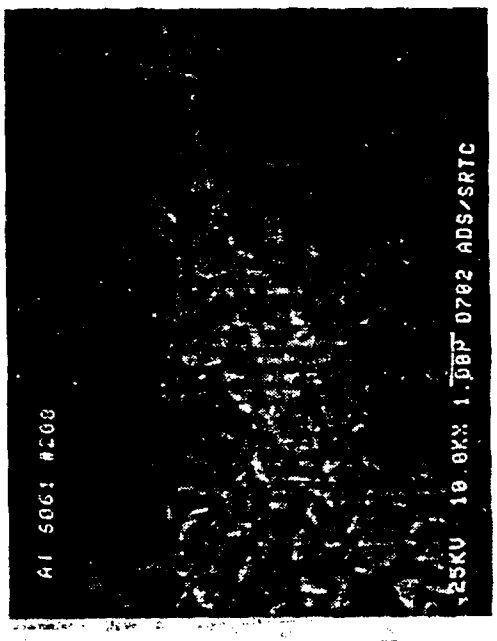

(d) 10,000X

Figure 22 - Aluminum 6061 Exposed To Gamma Radiation Field (High Magnification)

The following observations can be noted from a careful examination of the morphologies of the surface oxides of all three aluminum alloys:

- Aluminum 1100 - The blisters appear as empty rims. Smaller but closed (intact) blisters appear with continued exposure. The aluminum 1100 blisters are smaller than those in the other two alloys. The smooth background areas are covered with fine crystalline oxide.

- Aluminum 5052 - The number of blisters and the number of blisters with broken tops increase with exposure time. Very few open blisters have rims. The specimen surface is completely covered by blisters in eight weeks.

- Aluminum 6061 - The closed, broken, and rimmed blisters are present. Some open blisters have clusters of crystalline oxide inside. Other areas also show crystalline clusters. The specimen surface was not completely covered by blisters.

6.0 VAPOR CORROSION MECHANISMS

It has been shown that the gamma radiation field induced a different surface oxide morphology on the aluminum alloy surface. It may be an indication that the radiolysis has caused a slightly non-uniform or localized attack (Figs. 19 to 22), as opposed to a fairly smooth boehmite surface in a non-radiation field under condensate water vapor up to 200°C (Fig. 8). However, the basic water vapor corrosion mechanisms may be similar, except the corrosion rates are accelerated by the radiolysis effects.

Figures 23(a)* and 23(b) are, respectively, the cross-sections of alloy 1100 and 5052 samples with identical 200°C water vapor exposure history (no radiation) at which time the break-away corrosion of 5052 has already occurred (Fig. 4). It can be seen in aluminum 1100 (also in the case of aluminum 6061 but is not shown in this report) that the boehmite layers protected the metal substrate. However, the optical photograph in Figure 23(b) reveals channels and pockets or holes formed by internal oxidation of the metal substrate in aluminum 5052 with no gross microcracks and de-lamination of the surface oxide layer from the metal substrate. This discovery seems in contrast to a general explanation in the literature that microcracking and local de-lamination of the surface oxide provides a direct corrosion path between the environment and the bare metal and is responsible for break-away corrosion. A 300X (Fig. 24(a)) and a 4000X (Fig. 24(b)) SEM photographs confirmed that boehmite crystals appeared in the internal oxidation sites. The exposure time for these specimens was 2909 hours. The depth of attack for this aluminum 5052 specimen is about 160 μm.

* Figures 23(a,b) and 24(a,b) were obtained at the University of South Carolina at Columbia by Professor Anthony P. Reynolds in the Department of Mechanical Engineering under SCUREF (South Carolina Universities Research and Education Foundation) Task No. 212.

(a) Aluminum 1100 Substrate is Intact under the Oxide Film

(b) Internal Oxidation Occurred in Substrate Aluminum 5052

Figure 23 - Microstructures Of Pre- And Post Break-Away Corrosion
(Short Side of the Photographs is Approximately 180 μm)

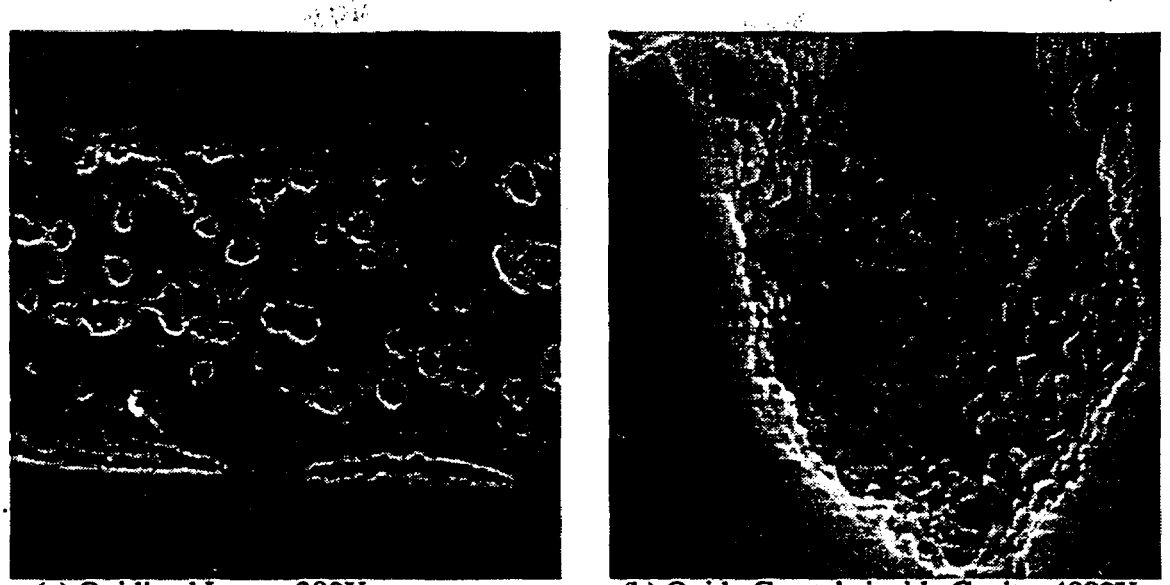

(a) Oxidized Layer, 300X (b) Oxide Crystals inside Cavity, 4000X

Figure 24 - Aluminum 5052 Internal Oxidation Morphology (SEM)

A set of optical micrographs taken earlier for oxide thickness evaluation (Table 5) was examined for evidence of the break-away corrosion. The specimen was under 200°C saturated water vapor for 1348 hours (autoclave test). From Figure 4, 1348 hours is about the time that the aluminum 5052 data begin to deviate from the parabolic corrosion curve, or alternatively, that time may mark the onset of the break-away corrosion of aluminum 5052. As shown in Figure 25, internal oxidation has just occurred. The figure also shows that the grain boundaries were under attack prior to the formation of the pockets or holes as in Figure 23(b) and 24(a,b). Although it is apparent that aluminum 5052 break-away corrosion is caused by internal oxidation starting along the grain boundaries, the root cause of internal oxidation in this alloy remains unclear. It appears that it may be linked to the high magnesium content and possible magnesium segregation to internal boundaries.

A similar attack can be seen in an aluminum 5052 specimen exposed to high gamma radiation field (about 1,810,000 R/hr) and initially saturated 200°C water vapor for one-week. The onset of internal oxidation is visible in Figure 26. It seems that the grain boundaries were again under attack prior to the formation of the internal oxidation sites.

As the internal oxidation of an aluminum 5052 specimen progressed to twelve weeks under a gamma radiation field of about 1,810,000 R/hr and initially 100% relative humidity, Figure 27(a) taken at 100X magnification shows that the internal oxidation sites are abundant along the specimen edges. The oxide layer on top of the metal substrate is visible and appears to be intact. At higher magnification (250X), Figure 27(b) shows that the internal oxidation is similar to that in Figure 23(b). It appears that the region of attack of metal progressed along the grain boundaries from the oxide-metal interface to the inner region of the alloy.

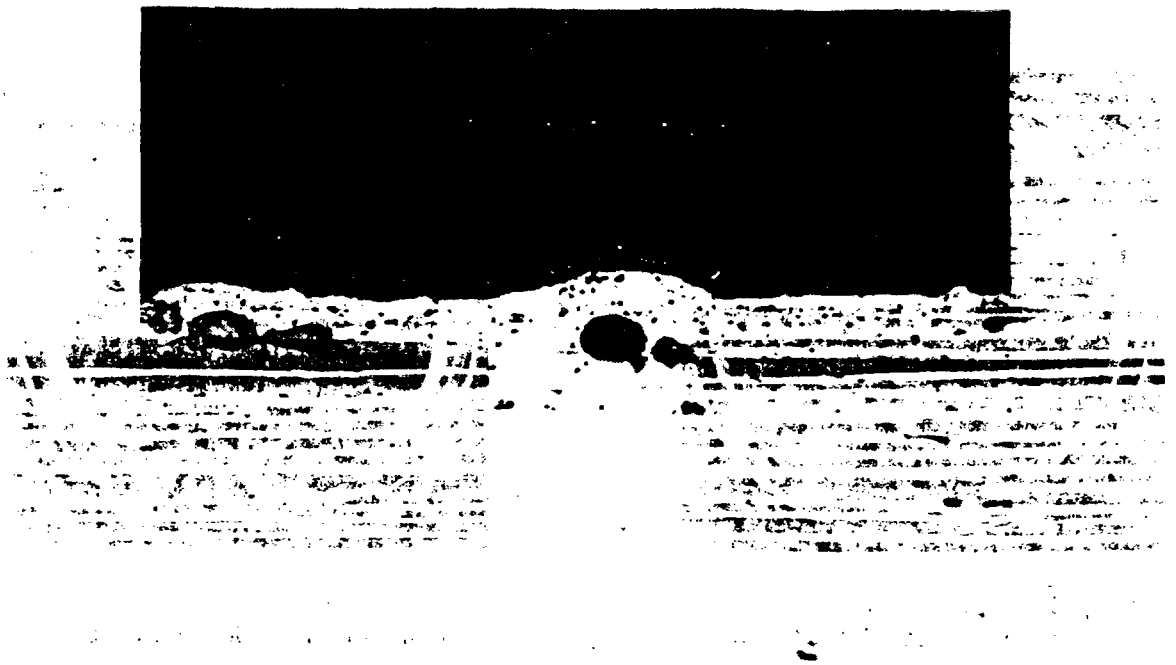

Figure 25 - Aluminum 5052 at the Onset of Break-away Corrosion in 200°C Water Vapor for 1348 Hours without Radiation Effects

(500X, Short Side of Photograph is 178 μm)

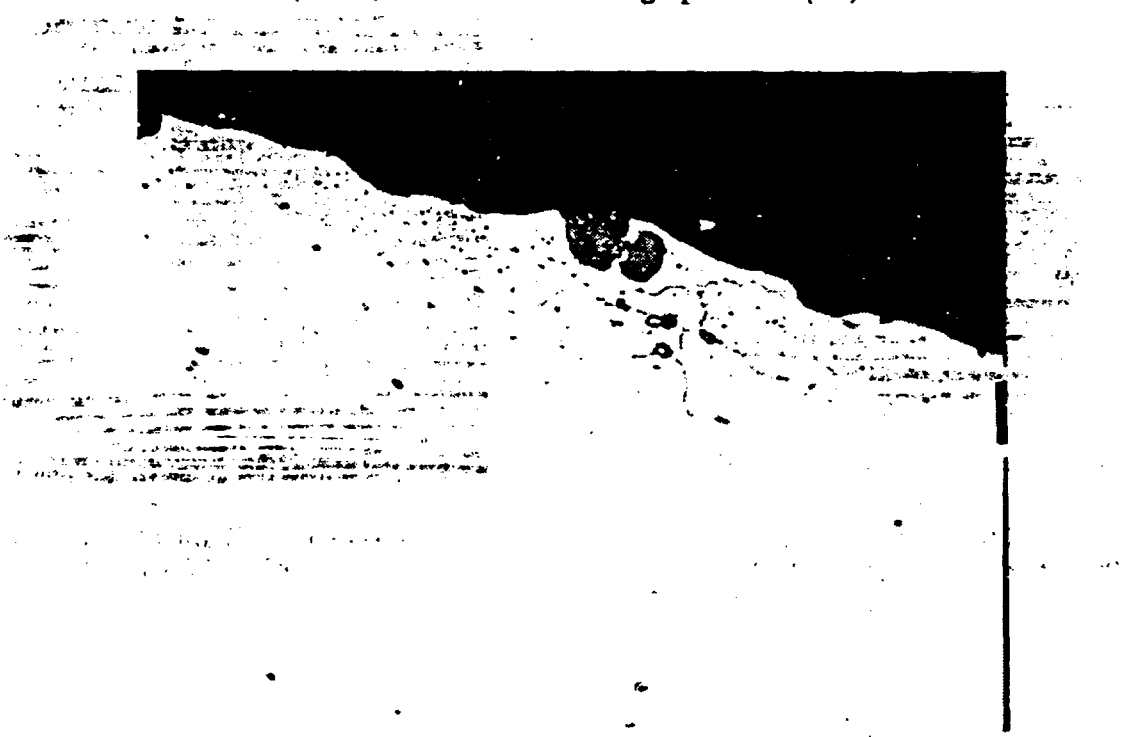

Figure 26 - Aluminum 5052 at the Onset of Break-away Corrosion under Radiation Field and 200°C Water Vapor for One Week

(500X, Short Side of Photograph is 178 μm)

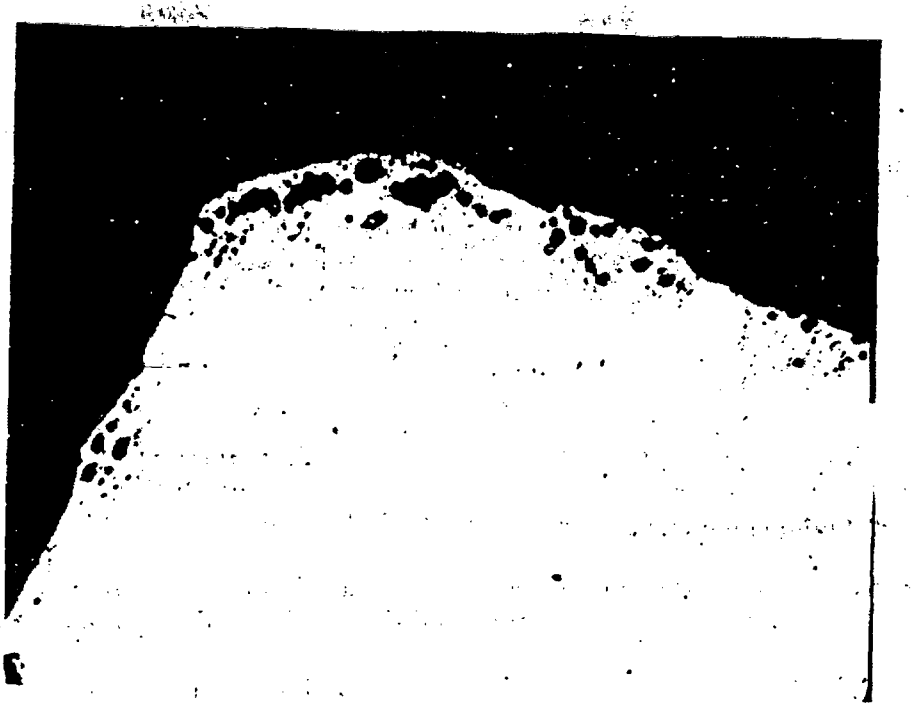

(a) Internal Oxidation in Aluminum 5052 (100X)

(b) Internal Oxidation in Aluminum 5052 (Short Side of Photograph is 356 mm, 250X)

Figure 27 - Internal Oxidation of Aluminum 5052 in Radiation Field and 200°C Water Vapor for 12 Weeks

On the other hand, there is no definite evidence of internal oxidation (pockets or holes) in aluminum 1100 and 6061 after twelve weeks of exposure to the same gamma radiation field and 200°C initially saturated water vapor. The corrodant seems to be consumed in the growth of a much thicker oxide (boehmite) films as shown in Figure 28, although these thick oxide layers appear only locally and do not cover over the entire metal surface. This thick oxide film was not observed in aluminum 5052 cross-sections.

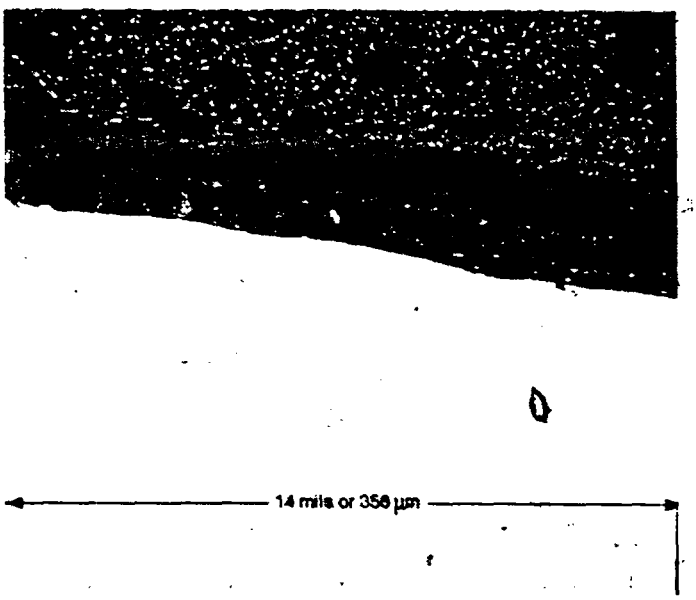

(a) Thick Oxide Film in Aluminum 1100 (250X, Oxide Thickness is about 50 µm)

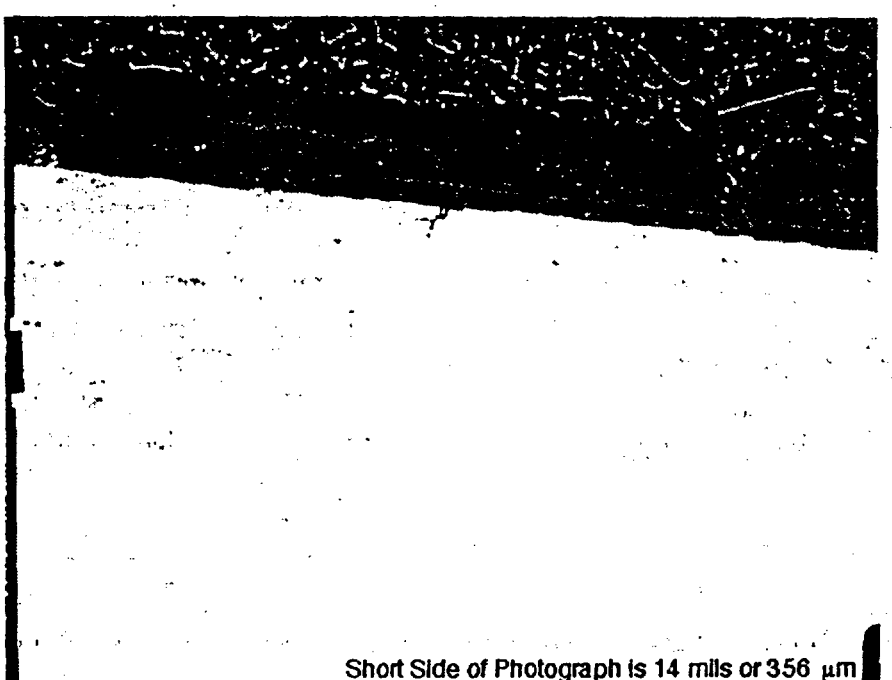

(b) Thick Oxide Film in Aluminum 6061 (250X)

Figure 28 - Thick Oxide Films in Aluminum 1100 and 6061 under Radiation Field and 200°C Water Vapor for 12 Weeks

Microcracks can be seen in the thick oxide layers as shown in Figure 28. According to the literature, these microcracks are responsible for the non-parabolic corrosion which includes break-away and paralinear corrosion (linear corrosion rate which is tangential to the initial parabolic corrosion curve). It is possible that paralinear corrosion may occur in the aluminum 1100 and 6061, once the oxide layers become thick enough and massive microcracks are formed to provide direct corrosion paths between the environment and the substrate metals.

Figure 29 shows a corrosion site below the oxide layer in aluminum 6061 after exposure to gamma radiation field for 12 weeks. The attack appears to follow the grain boundaries but further characterization is required to determine if it is the same mechanism as that in the case of aluminum 5052. Note that aluminum 6061 also contains magnesium at a concentration about 1 wt% less than that in the aluminum 5052 (Table 1).

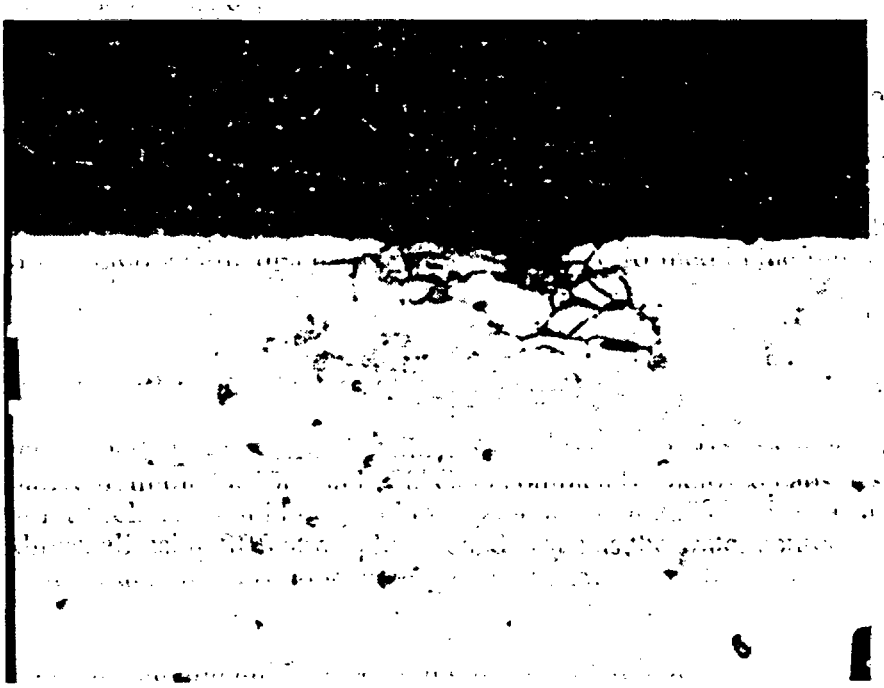

Figure 29 - Corrosion Site near the Oxide Layer in Aluminum 6061 under Radiation Field for 12 Weeks (250X).

7.0 VAPOR CORROSION OF FUEL MATERIALS - ALUMINUM-URANIUM ALLOYS

Most of the FRR/DRR fuels to be returned to SRS are UAl_x fuel. The fuel material will be subject to vapor corrosion when the aluminum cladding is penetrated or consumed. The corrosion products and their behavior will be input to the waste form performance studies for the direct disposal of spent nuclear fuels.

Aluminum-10 wt% uranium alloy was tested in an autoclave at 200°C under saturated vapor. Two types of specimens were used: 1) Coupon specimens which were heavily hot rolled to sheets and then cut to a rectangular shape (2 inches x 0.75 inches x 0.125

inches) similar to the aluminum alloy coupons used throughout this corrosion program; 2) Disk specimens which were made by cutting an extruded rod with diameter 0.624 inches and thickness 0.051 inches. These two sets of specimens were tested separately in the autoclave at 200°C and 100% relative humidity. The specimens were taken out of the autoclave at intervals for weight gain measurement up to exposure times of 1500 to 1700 hours (about 70 days).

Aluminum-18 wt% uranium and aluminum-33 wt% uranium are more representative of the high enriched and low enriched FRR/DRR fuels than the aluminum-10 wt% uranium. Plans have been made to perform additional coupon tests with specimens of these compositions.

Results of Vapor Corrosion of Aluminum-Uranium Alloy

Figure 30 shows the weight gain curves for the coupon specimens and the disk specimens. The initial corrosion was specimen dependent with a large range in weight gain. However, the corrosion rates (the slopes of the curves) appear to be consistent. The corrosion rates differ slightly between the coupon specimens and the disk specimens. Nevertheless, all the weight gains for the aluminum-10 wt% uranium coupon specimens are much higher than those for aluminum 1100 with the same exposure time at 200°C. The aluminum 1100 weight gain is comparable to those for disk specimens No. 7 and No. 8, which are the lower bound of the data shown in Figure 30. Reasons for the large range in the initial weight gain are unclear and remain to be investigated. The microstructural inhomogeneity of the alloys may be a factor.

Micromechanisms of Vapor Corrosion of Aluminum-Uranium Alloys

Metallography shows that the hot rolled specimens (coupons) and the extruded specimens (disks) have different microstructures (Fig. 31). Large areas of eutectic between elongated bands of primary aluminum can be seen in the extruded specimens. Broken fragments of UAl_x (most likely UAl_4 for the 10 wt% of uranium alloy) are scattered in the aluminum matrix in the hot rolled specimens. These observations account for the different corrosion rates. However, the actual mechanisms causing the discrepancy have not yet been determined.

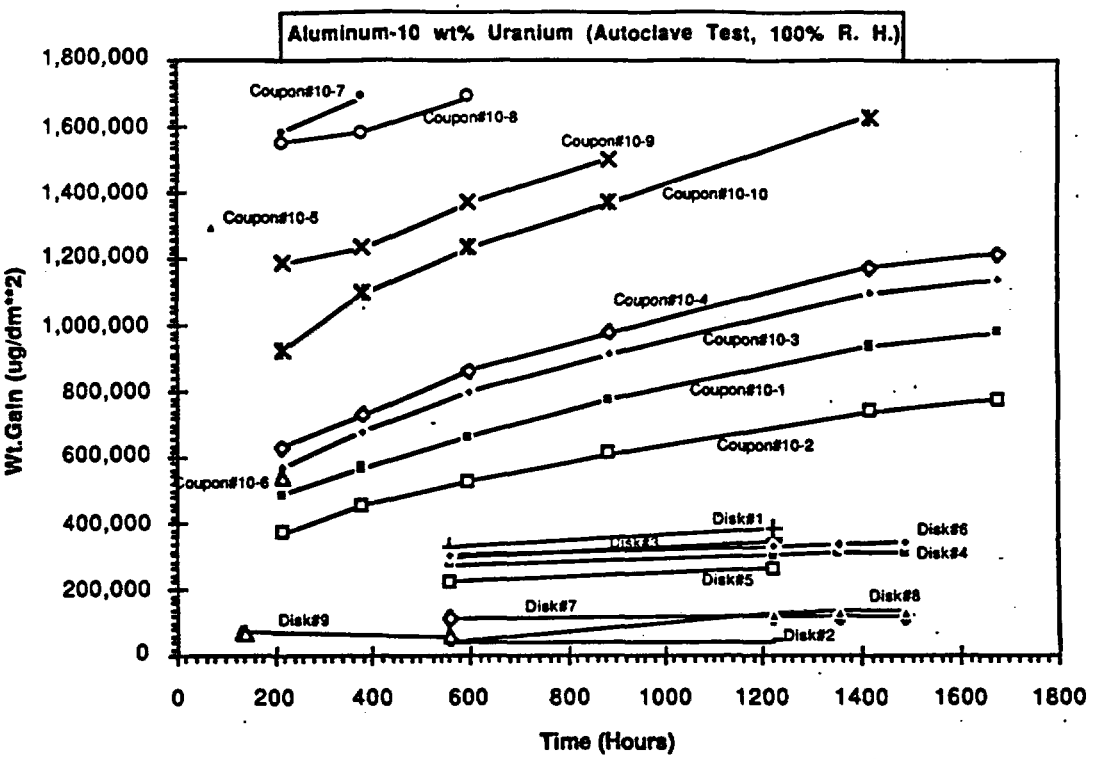

Figure 30 Corrosion of Aluminum-10 Wt% Uranium Alloy at 200°C in Saturated Water Vapor

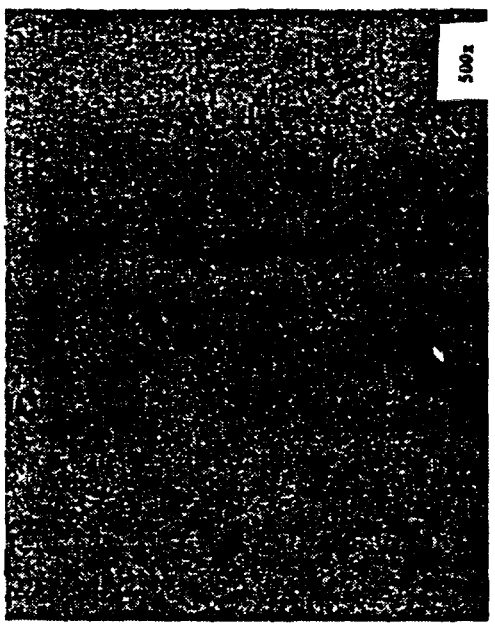

(a) Hot Rolled Aluminum-10 wt% Uranium Alloy in Longitudinal Direction

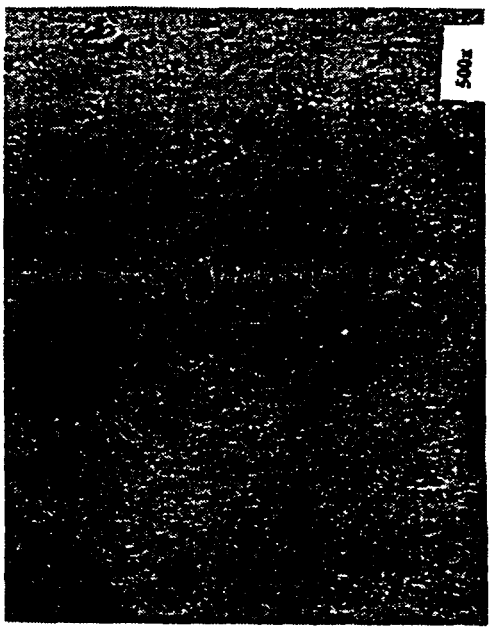

(b) Hot Rolled Aluminum-10 wt% Uranium Alloy in Transverse Direction

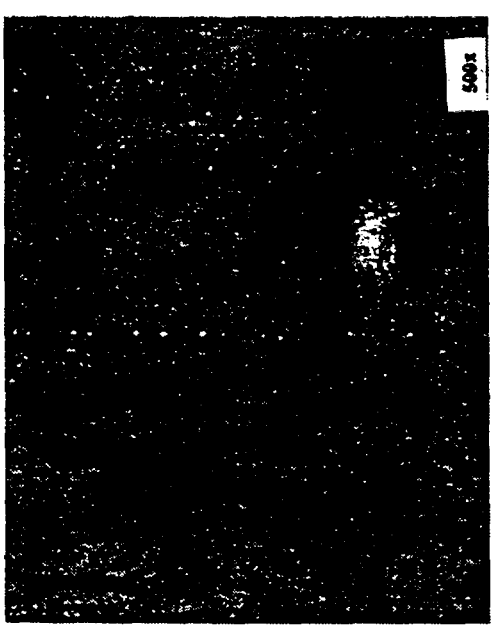

(c) Extruded Aluminum-10 wt% Uranium Alloy in Longitudinal Direction

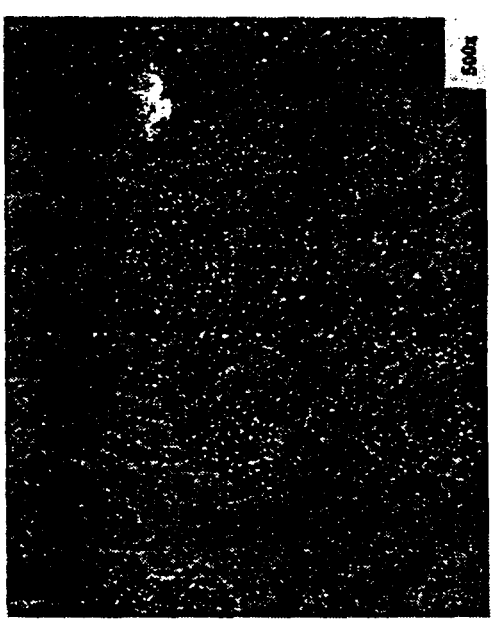

(d) Extruded Aluminum-10 wt% Uranium Alloy in Transverse Direction

Figure 31 - Microstructures of Hot Rolled And Extruded Aluminum-10 Wt% Uranium Alloys

Severe corrosion accompanied by blistering has been noticed in the hot rolled specimens. Optical and scanning electron microscopic photographs were focused on a blistered area in a specimen with only four days of exposure (Figure 32). It shows a blistered region covered by a thick oxide layer. In addition, a large number of uranium aluminide particles are scattered in the metal matrix as well as in the oxide layer. This indicates that the uranium aluminide is more stable than aluminum and does not react or reacts very slowly in the 200°C saturated vapor environment.

The aluminum-10 wt% uranium was used for initial testing of Al-U alloys. As noted earlier, typical fuel materials for FRR and DRR are aluminum-18 wt% uranium and aluminum-33 wt% uranium. The microstructures of these two alloys are shown in Figure 33. It is obvious that UAl_4 and UAl_3 are the major block-like particles, respectively, in the 18% and 33% uranium alloys. They also notably differ from the aluminum-10 wt% uranium in Figure 31. It is expected that the corrosion behaviors will differ. Further tests with these alloys are being planned.

8.0 PITTING CORROSION OF AL-U ALLOYS IN WATER VAPOR

Artificial pits were milled in the cladding of coextruded fuel tubes (Figs. 34(a) and 34(c)) of aluminum-18 and -33 wt% uranium fuel clad with 0.030-inch thick aluminum 8001 alloy. Various pit sizes were chosen (1/32, 1/16, and 1/8 inches in diameter) and for each pit size the depths of the pits were 0.010, 0.020, 0.025, and 0.031(through-clad) inches. Optical metallography was employed to confirm the pit depths.

These ring-shaped specimens were placed in an autoclave at 200°C in saturated water vapor. Another set of the pitting specimens were put in capsules with 20% and 100% relative humidity and tested in 150°C ovens. Nitric acid solution was used for some capsules to simulate the effects of a radiation environment.

Results of Vapor Corrosion- U-Al Alloy, Pit Specimen

The pitted areas of the 200°C autoclave specimens were sectioned and examined by optical metallography. No penetration by oxidation was found in areas with 0.005 inch residual cladding (corresponding to a pit with a depth of 0.025 inches). For pits machined to penetrate the cladding, uneven oxide was formed in the bottom of the pit, while the oxide layers on the sides of the pits were uniform.

In the autoclave specimens with two-month exposure to saturated water vapor at 200°C, corrosion occurred only in the initially exposed aluminum-uranium core, that is, in the two ends of the samples (Fig. 34(b)) and in the through-clad pits (Fig. 34(d)). The black corrosion product was stripped from the pits and was determined by XRD as a mixture of U_4O_9 and boehmite ($Al_2O_3 \cdot 3H_2O$).

The capsule test at 150°C in a water vapor environment for 12 months showed a similar result. In the case of capsules with 20% relative humidity, the degree of oxidation was markedly reduced. However, more pits were found to contain the black oxide in the capsule containing nitric acid and 100% initial relative humidity.

(a) Optical Microscopy

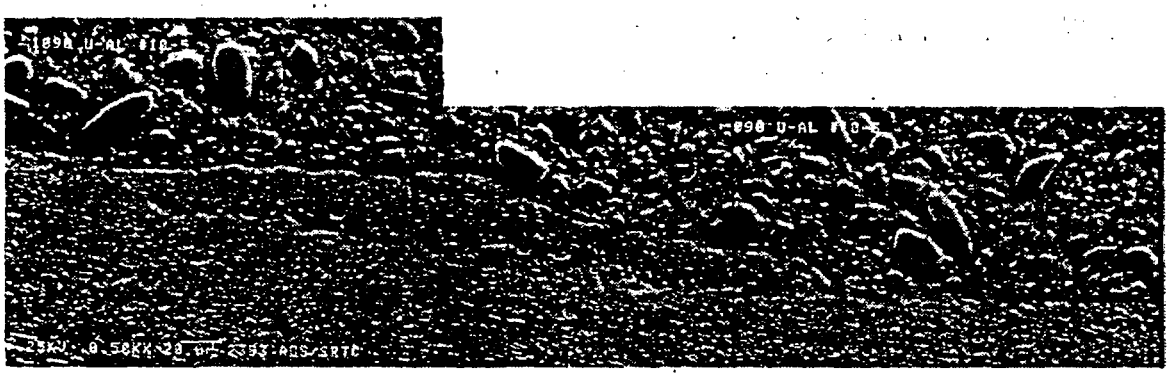

(b) Scanning Electron Microscopy

Figure 32 - Optical and SEM Photographs of a Blistered Area in Aluminum-10 wt% Uranium Hot Rolled Alloy under 200°C Saturated Water Vapor for Four Days. (500X)

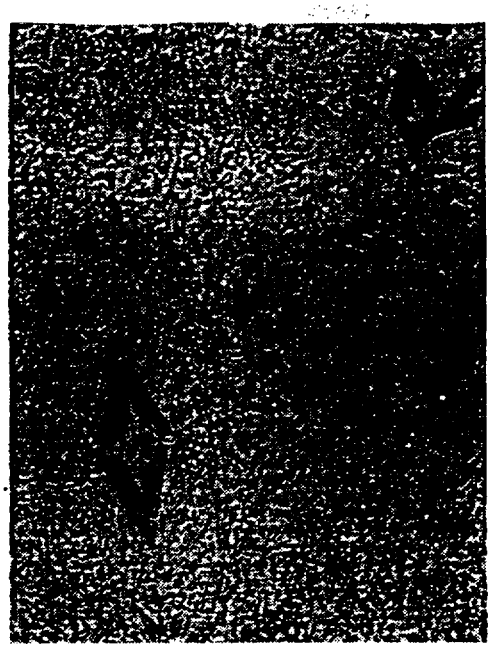

(a) Aluminum-18 wt% Uranium in Longitudinal Direction (500X)

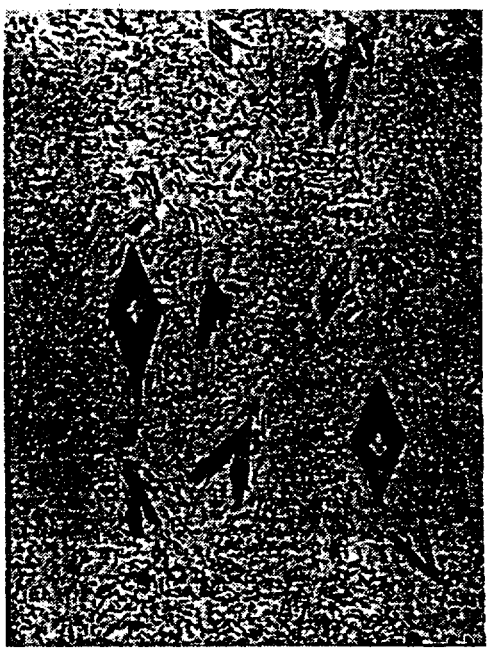

(b) Aluminum-18 wt% Uranium in Transverse Direction (500X)

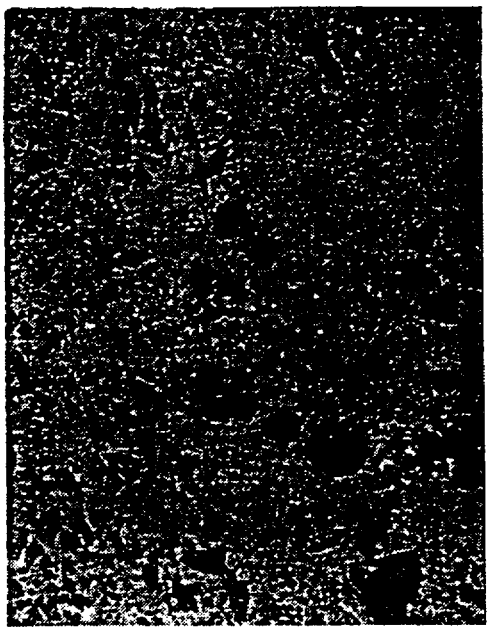

(c) Aluminum-33 wt% Uranium in Longitudinal Direction (500X)

(d) Aluminum-33 wt% Uranium in Transverse Direction (500X)

Figure 33 - Microstructures of Aluminum-Uranium (18 & 33 wt%) Alloys

(a) As Received Fuel Tube showing Aluminum 8001 Cladding and Aluminum 18 wt% Uranium Core

(b) Corroded Specimen in a Capsule with Initial 100% R. H. Water Vapor and Nitric Acid at 150°C after 12-Month Exposure

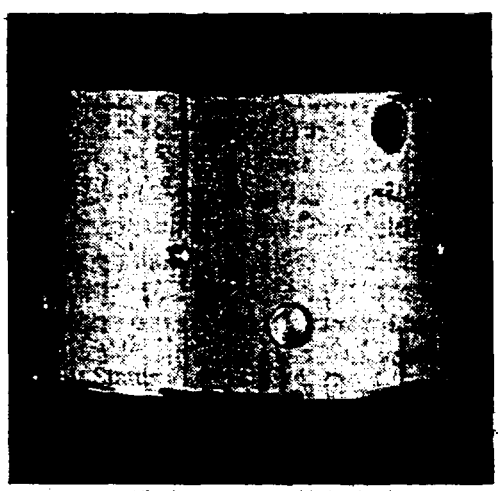

(c) Typical Ring Specimen (Fuel Tube) with Artificial Pits

(d) Black Oxide Formed in a Pit with 1/8" Diameter Exposed to 100% R. H. Water Vapor

Figure 34 - Typical Ring Specimen (Fuel Tube) and Pitting Corrosion

9.0 HYDROGEN GENERATION IN A CLOSED SYSTEM

When the aluminum cladding alloys interact with water vapor, hydrogen gas is generated along with the aluminum oxides (for example, boehmite). The reaction equation can be found in Section 3.0. The generation of hydrogen will stop if the corrodant species (water) is depleted. Therefore, in a closed system such as in a test capsule or in a sealed spent nuclear fuel canister, the total amount of hydrogen that can be produced by corrosion and the corresponding hydrogen pressure can be estimated by the ideal gas law and the weight gain equations. It can be shown that

$$P_{hydrogen} = \frac{1}{V}\frac{m_h}{2}RT$$

where $P_{hydrogen}$ is the pressure of the hydrogen gas, V is the air space or free volume of the closed system, m_h is the mass of hydrogen generated, R is the universal gas constant (R = 8.314 J /g•mole•K or N •m/g•mole•K), and T is the absolute temperature (K).

The amount of hydrogen generated, m_h, can be expressed in terms of the weight gain of the specimen. Assuming the oxide form is boehmite,

m_h = (6/66) x (Weight Gain), and
Weight Gain = (weight gain equation in terms of unit area and time) x (specimen surface area)

For example, the weight gain equations in Section 3.0 for aluminum alloys 1100, 5052, and 6061 (or equivalently, their pure power law corrosion models) were used to generate Figure 35 for a test capsule with 70 ml volume and containing three standard specimens at 150°C with initial relative humidity of 100%. The use of the corrosion models developed on the basis of unlimited corrodant scenario (autoclave test) is conservative. Figure 35 also includes the change of water vapor pressure and relative humidity. The calculation of water pressure requires the input of steam table data (vapor pressure as a function of specific volume). The relative humidity is defined as the percentage of vapor pressure in terms of the saturation pressure at the temperature. For example, the saturation pressure for 150°C vapor is 69.046 psia. The total pressure inside the capsule is the sum of the water vapor pressure, the hydrogen gas pressure, and the air pressure.

It can be seen in Figure 35 that the hydrogen pressure rises as the water vapor pressure decreases. The process stops in about 5.6 years when all the water is consumed by the corrosion reaction. The total pressure is actually less than its initial value which is the saturation pressure of water vapor at 150°C. This calculated decrease in total pressure may not be valid when nitric acid or radiolysis is present. The gas generation in systems other than water vapor must be characterized.

In the capsule tests that have been carried out, it was observed that the opened capsules after exposure were dry or contained very little moisture. This is a direct evidence of water depletion as a result of oxidation of the aluminum.

The specimens in the capsule tests showed growth of a boehmite layer under all air/water vapor/temperature conditions of exposure. There was no evidence that dehydration of the boehmite layer occurred under the high radiation field ($2x10^6$ R/hr) up to 200°C for twelve weeks. It is assumed that the hydrated water in the boehmite ($Al_2O_3•H_2O$) is not

freed by radiolysis and therefore is not available for further corroding the aluminum cladding alloys and generating hydrogen gas. This assumption will be investigated in a future test.

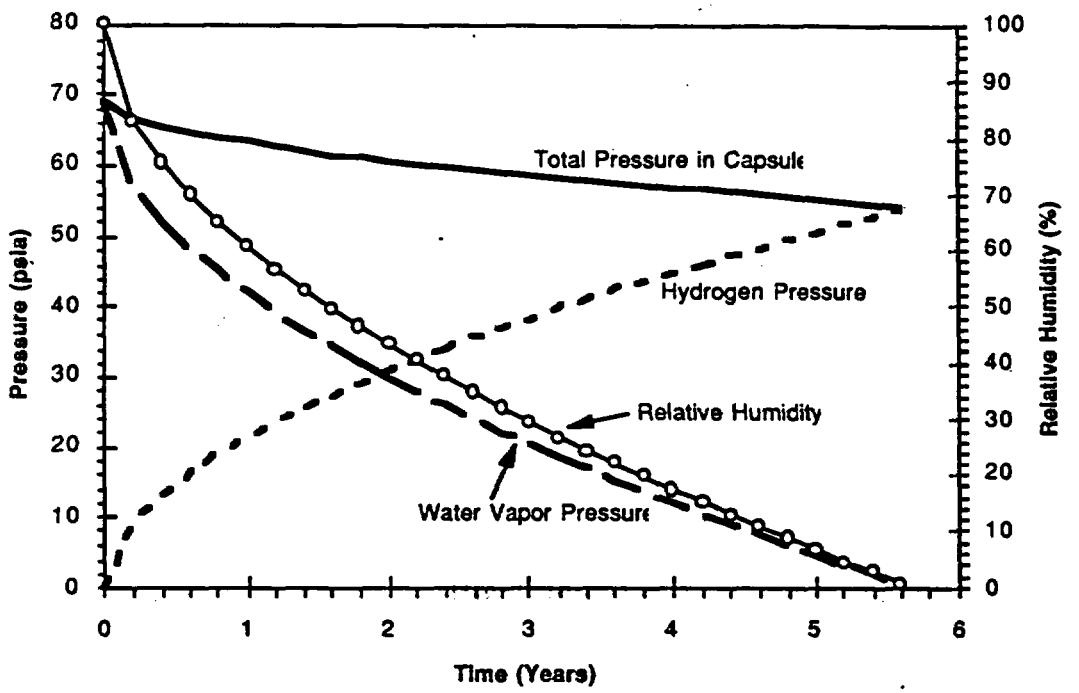

Figure 35 - Hydrogen Generation and Pressure Changes in a Closed System at 150°C

10.0 APPLICATIONS TO STORAGE SYSTEMS

(1) Application to Interim Dry Storage or Road Ready Package:

The fuel will most likely be stored in a sealed system. Limiting the hydrogen generated in a sealed system to 4% by volume will prevent the potential for explosion. The amount of water or the degree of dryness for this system can be calculated based on the chemical reaction equation which conservatively assumes that boehmite is formed on the aluminum alloy surface:

$$2\,Al + 4\,H_2O \;\text{---}> \; Al_2O_3{\cdot}H_2O + 3\,H_2$$

Assuming all the water will be consumed by oxidation, the maximum allowable water (W_{water}, in grams) is expressed as a function of the free volume (V, in cm^3) of the container:

$$W_{water} = 3.873 \times 10^{-5}\,V$$

in which the molar volume of hydrogen, 24789.2 cm^3, was used.

With the allowable amount of water calculated, the initial relative humidity of the system can be obtained at the specified operating temperature.

In theory, the result of a capsule test at that relative humidity can be used to estimate the cladding corrosion rate. However, the application of the corrosion models (Section 3.0) developed with the autoclave test data at a constant 100% relative humidity will lead to a conservative estimate of cladding corrosion. The time required for a complete loss of cladding materials is expected to be much longer than the specified time allowed for interim dry storage or in a road ready package. Additional credit can be taken for the integrity of the cladding materials.

(2) Application to the Repository:

For a breached overpack and spent nuclear fuel canister, and under vapor and/or aqueous conditions, the aluminum cladding would be expected to be eventually convert to hydrated oxides. Next the core would be expected to convert to hydrated oxides of aluminum with the fuel particles (e.g. UAl_x) possibly remaining stable. Thermodynamic analysis will be performed for expected chemistry and environmental conditions to predict the range of possible forms of the corroded fuel. Experimental investigation of the stability of the intermetallic fuel particles will also be performed in the future corrosion testing of the fuel materials.

11.0 CORROSION PROGRAM - PATHFORWARD

Tests have been carried out for aluminum alloys 1100, 5052, and 6061 in an autoclave with 100% relative humidity at 150° and 200°C, in completely enclosed capsules at 150°C with various relative humidities, and in a gamma cell at 200°C with various relative humidities, all using SRS atmospheric condensate as the water source. Capsule tests at 200° (with water and nitric acid solution) and at 250°C (with water only) are in progress.

For the fuel materials, aluminum-10 wt% uranium was tested in an autoclave at 200°C and in capsules at 150°C. Weight gain data show specimen-to-specimen variations larger than expected considering the aluminum alloy results. Metallographic examinations are needed to explain the possible role of microstructural variations between the hot rolled and extruded specimens on the corrosion mechanism. Tests for typical fuel materials such as aluminum-18 and -33 wt% uranium alloys should be carried out to obtain relevant corrosion data for FRR/DRR fuels.

Additional cladding and fuel materials will be tested at several relative humidities in a gamma radiation field with the J-13 well water chemistry as the water source. It is expected that the J-13 water vapor would cause a higher corrosion rate, since the water chemistry contains chloride which is an aggressive corrodant species. Constant 100% relative humidity capsules should be included to establish the upper bound on the corrosion rate for an air/water environment in the presence of a radiation field. The correlation between the nitric acid test and the gamma cell test will be investigated. The

species resulting from the radiolysis of water vapor should be identified for input to radioactive performance assessments and for criticality analyses.

The corrosion models should be refined to include the humidity and radiation effects, if sufficient data are available. This will broaden the applicability of the model to cover both the interim dry and repository environments. The corrosion products will be examined to identify stable phases of aluminum-uranium alloys so that performance assessment and criticality analysis may benefit from the information.

12.0 REFERENCES

1. H. P. Godard, "Oxide Film Growth Over Five Years on Some Aluminum Sheet Alloys in Air of Varying Humidity at Room Temperature," J. Electrochemical Society, Vol. X, p. 354, 1967.

2. W. H. J. Vernon, "A Laboratory Study of the Atmospheric Corrosion of Metals," Trans. Farad. Soc.; Vol. 27, p. 255, 1931.

ACKNOWLEDGMENTS

Tracy H. Murphy is greatly appreciated for performing all corrosion tests and maintaining records of test data and equipment calibration. Special thanks to R. Ross Lathrop for setting up equipment; and to Dr. George R. Caskey, Jr. for interpretation of micrographs and useful discussions of corrosion mechanisms. Gamma cell engineering and test support from Ronnie E. Long and test capsule welding support from David N. Maxwell, Sr. are gratefully acknowledged.